Search for WIMP Dark Matter with the ATLAS Detector in the Monojet Channel: Run 1 Results

Noah Kurinsky

SASS, April 20, 2016

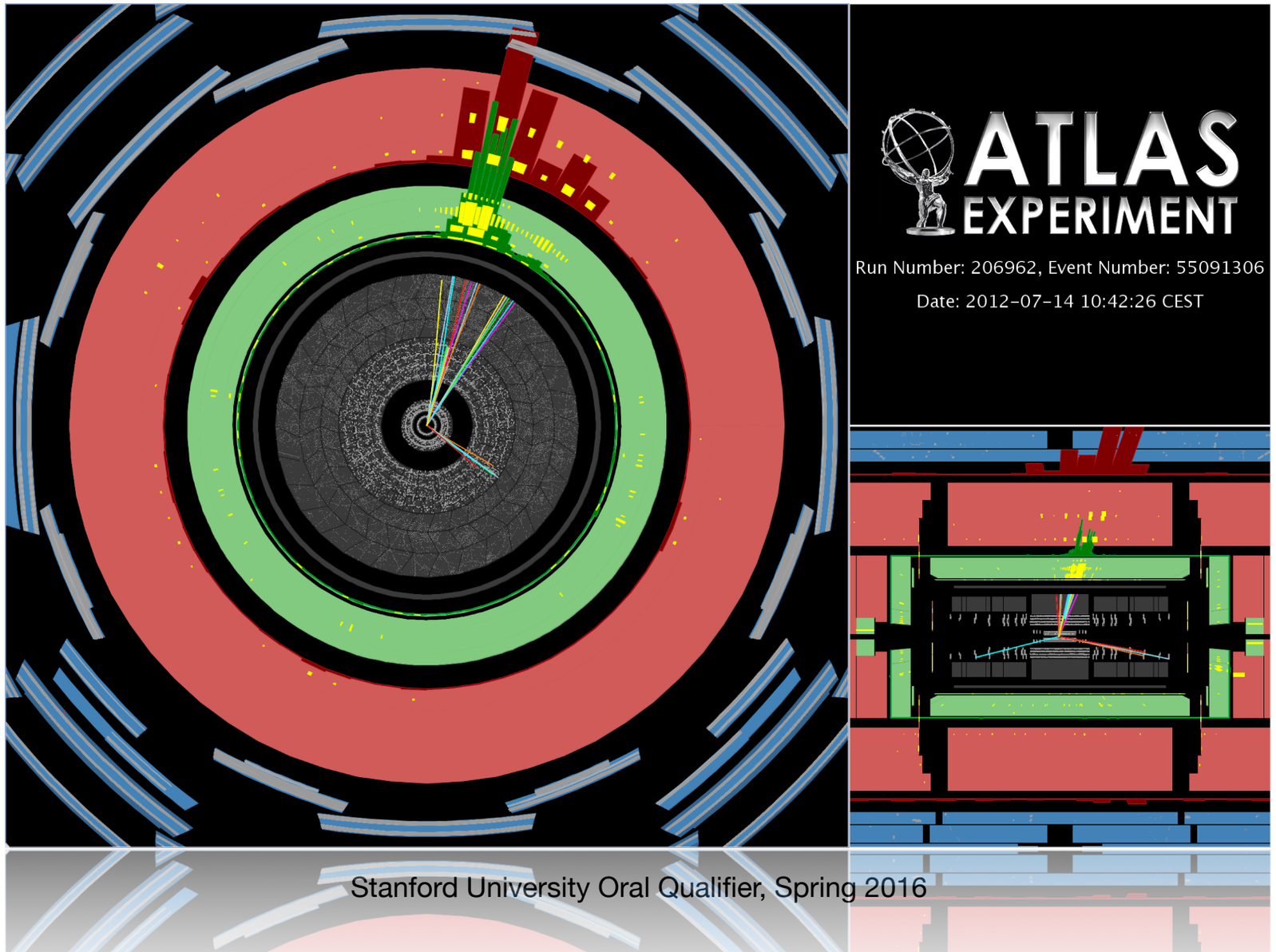

Talk Outline

- Motivation
  - Existence of Dark Matter
  - Need for BSM Physics
  - Thermal Relic Abundance
  - Complementarity with Direct and Astrophysical Searches
- Theoretical Framework
  - Motivation from Supersymmetry and other BSM Theories
  - Effective Field Theory of Dark Matter Interactions
  - Sensitivity of LHC Detectors to EFT Operators
  - Single Massive Mediator BSM Extension
- Experimental Setup
  - The ATLAS Detector and *pp* Event Reconstruction
  - BSM Physics in the Monojet Channel
  - Expected backgrounds
  - Signal and Background Simulations
- Results and Conclusions
  - Signal Measurement
  - Limits on mediator mass
  - Comparison to direct and indirect cross-section limits
  - Future Prospects (Run 2 and beyond)

Motivation

- Existence of Dark Matter
- Need for BSM Physics
- Thermal Relic Abundance
- Complementarity with Direct and Astrophysical Searches

Initial Hints: Galaxy Kinematics

- In 1933, Fritz Zwicky calculates that the Virial mass of the Coma cluster was far in excess of the visible matter
- In the 60's and 70's, Vera Rubin and Kent Ford show that all galaxies have flat rotation curves, which cannot be explained by their visible matter distribution
- The combination of the viral theorem, with the assumption of a flat rotation curve, implies that total mass increases proportional to the enclosed radius, a trend opposite to what we observe in light
- Until observation of non-kinematic evidence, MOND and other modified gravity theories seemed equally likely as explanations

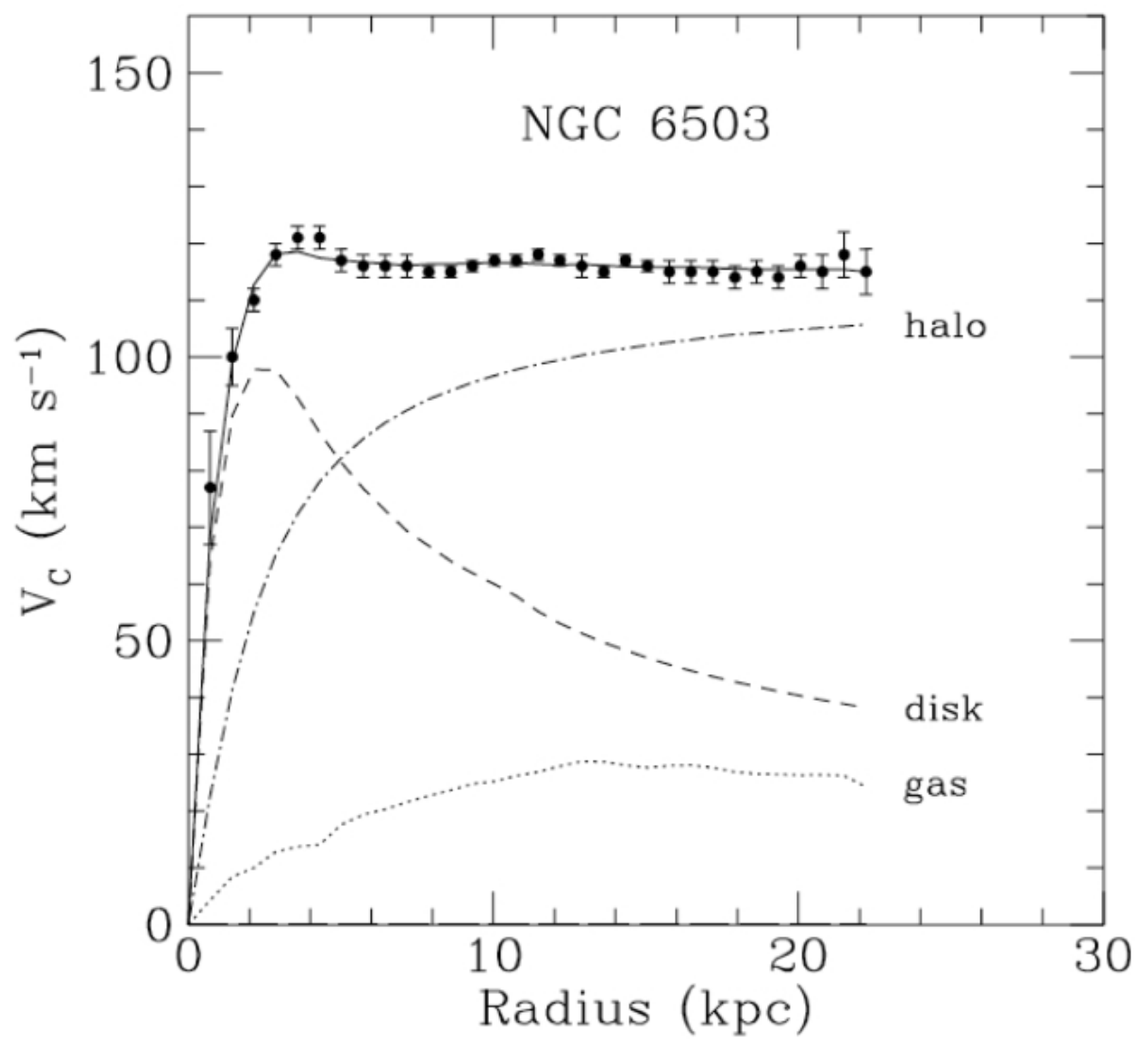

http://www.astro.queensu.ca/~courteau/Phys216/kin.html

Astrophysical Evidence for Dark Matter

- Today, dark matter is required to explain gravitational phenomena across many cosmic scales
  - Simulations cannot produce stable galaxies in the lifetime of the universe without substantial contributions from cold dark matter
  - Gravitational lensing, notably that in the bullet cluster, shows separation between gravitational potentials the distribution of observable matter in systems of interacting galaxies
  - Dark matter is needed to explain the apparent structure deduced from CMB anisotropies

- Dark matter is so integral to cosmology that it defines our standard cosmological model, which we call the Lambda-CDM (Cold Dark Matter) model, and drives early galaxy evolution

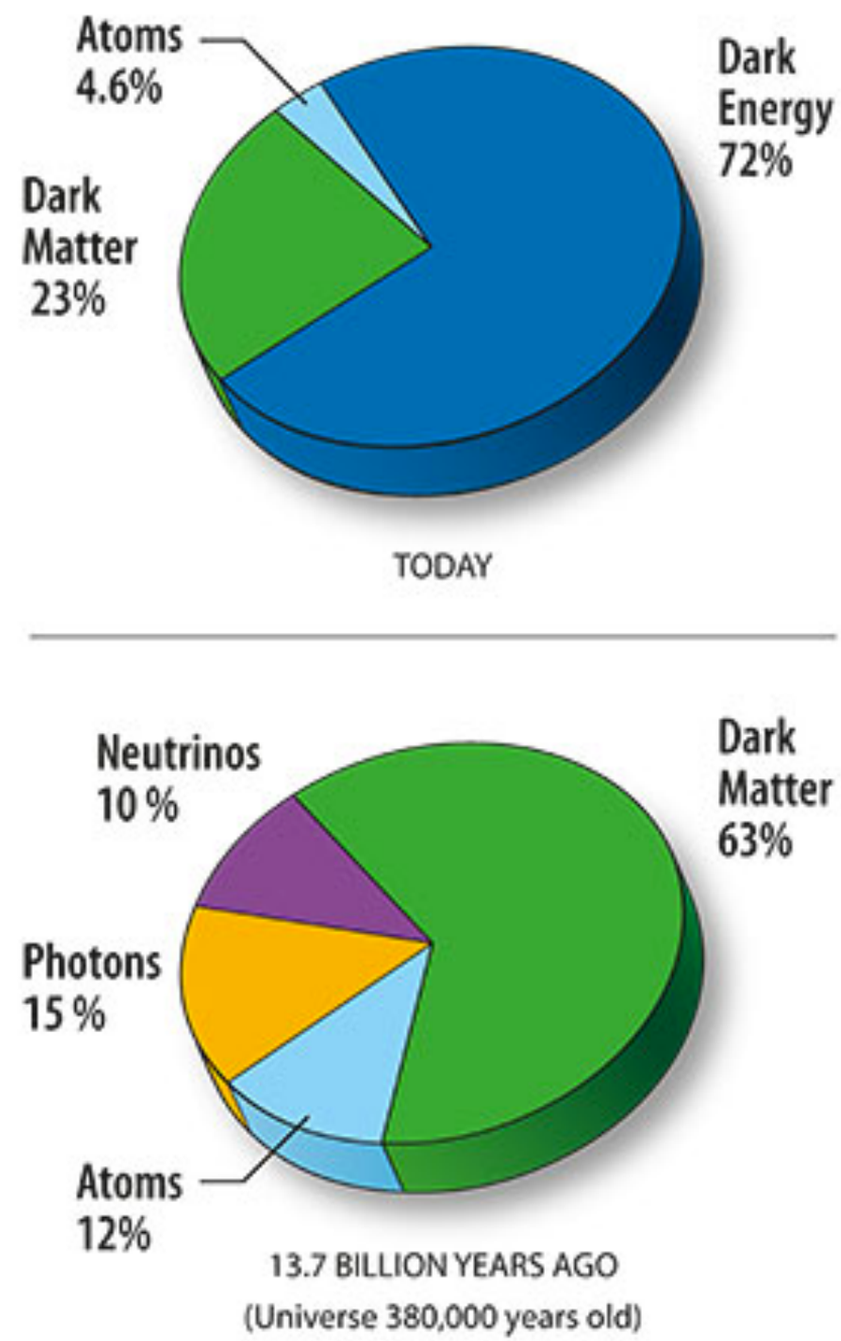

Motivation: Physics Beyond the Standard Model

- The Standard model of particle physics has been successful at describing many quantum phenomena and low-energy processes (e.g. atomic decay, spin) but many unsolved theoretical problems remain aside from astrophysical motivations:
  - Matter/Antimatter Asymmetry
  - Neutrino Masses and Neutrino Oscillations
  - Incorporation of Gravity
  - Fine-Tuning (Naturalness)

- The introduction of many new theories intended to solve these problems naturally introduces additional particles, and thus searches in channels which the SM predicts to be quiet are a good probe of BSM physics
  - SUSY predicts LSP, stable dark matter candidate
  - Axions also potential ultra-light DM candidate

- A good dark matter candidate just needs to be the lightest of a new class of particles without a lighter candidate to decay to, thus almost all BSM theories admit interesting dark matter candidates

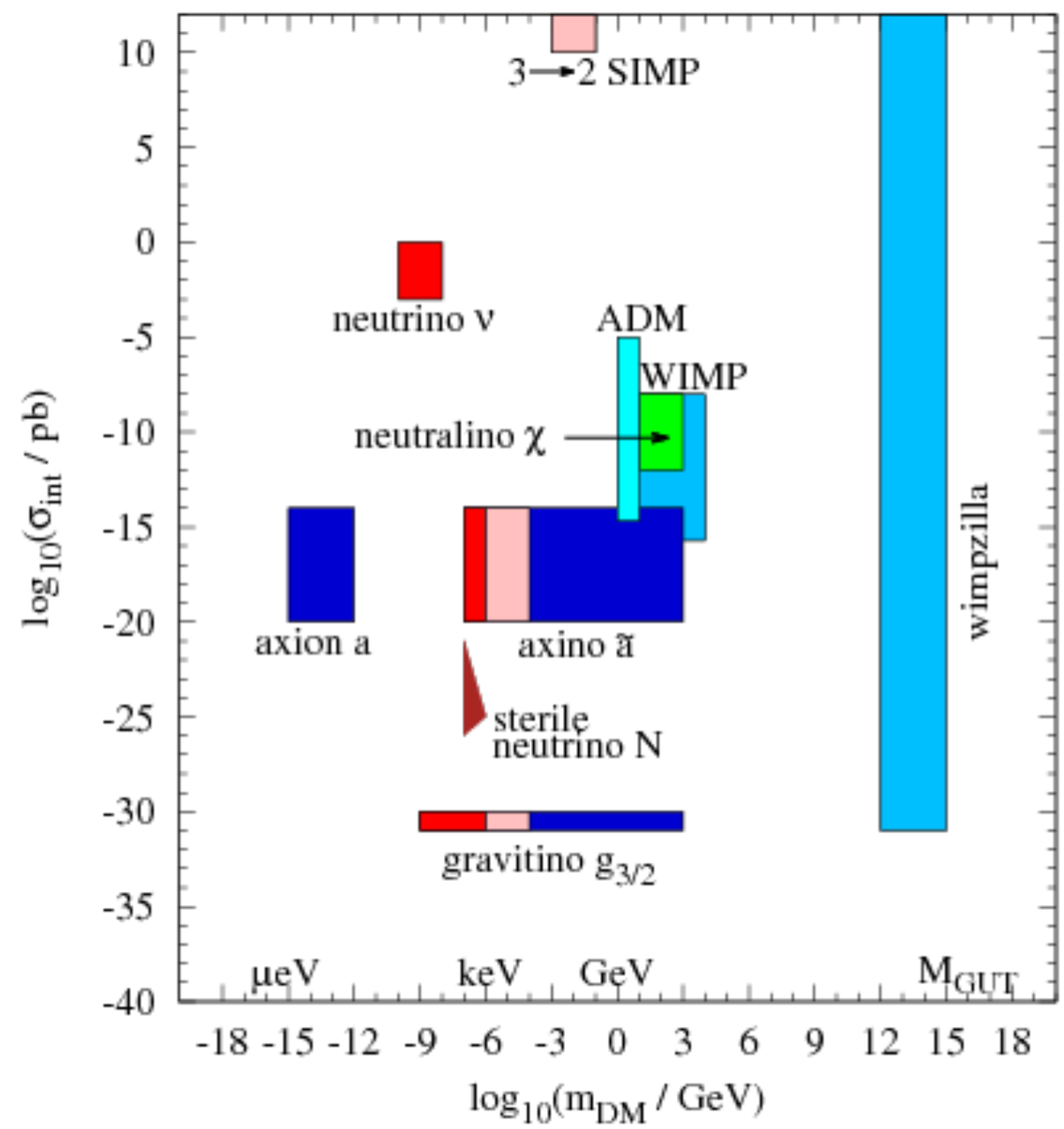

Thermal Relic Abundance

- The measured relic abundance from Planck is ~0.26, and we find that the predicted relic abundance is given by the relation

$$\Omega_M \propto \frac{m_\chi^2}{g^4}$$

- Much excitement in recent years came from two developments:
  - WIMPs with mass in the 10 MeV - 10TeV range shown to produce roughly the correct thermic relic abundance
  - DAMA and CoGent announced possible WIMP detections near the sweet-spot

- The natural parameter space which initially caused the excitement has been ruled out, but much of the space remains allowed, if not slightly less "miraculous"
  - The WIMPless miracle may also allow for dark matter with these properties in a supersymmetric framework (http://arxiv.org/pdf/0803.4196v3.pdf)

Feng and Kumar 2008

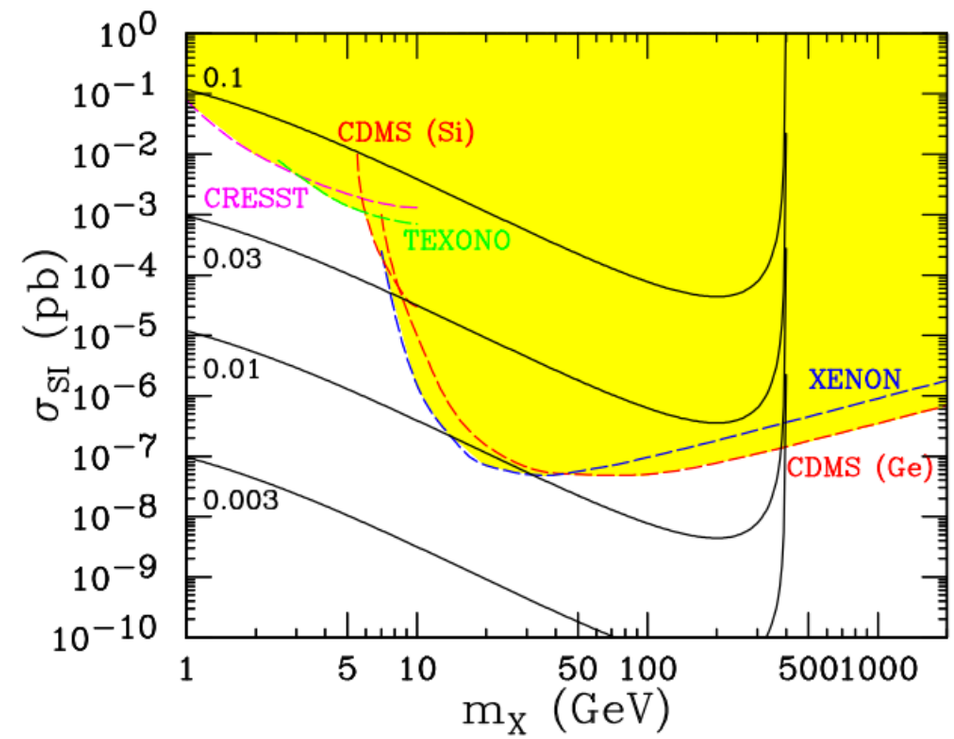

FIG. 2: Direct detection cross sections for spin-independent X-proton scattering as a function of dark matter mass m_X. The solid curves are the predictions for WIMPless dark matter with connector mass $m_{Y_u} = 400$ GeV and the Yukawa couplings λ_u indicated. The shaded region is excluded by CRESST [18], CDMS (Si) [19], TEXONO [20], XENON [21], and CDMS (Ge) [22].

Advantage of DM in Colliders

- Collider searches are one of the three time-slices of the four-point DM/SM interaction diagram
- Indirect searches rely on secondary observables and are limited by complex backgrounds
- Direct searches are limited by low momentum transfer from cold dark matter, and fixed background density
- Collider searches can dial up the intensity and overwhelm the backgrounds

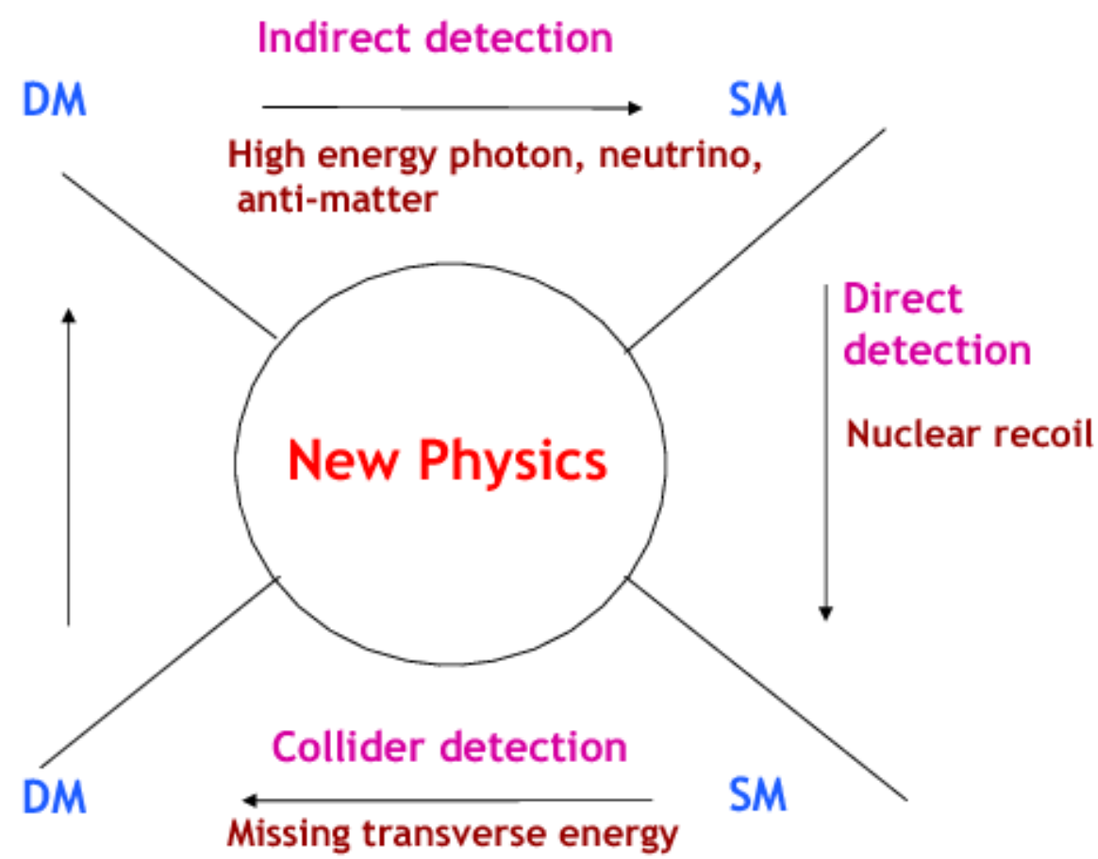

Theoretical Framework

- Hadron Collisions at the LHC
  - Initial and Final States
- Effective Field Theory of Dark Matter Interactions
- Single Massive Mediator BSM Extension

Standard Model Detector Signatures: Initial States

- Particle colliders actually collide particle "bunches"
  - Each bunch has ~100 billion protons, with crossing time of ~25 nanoseconds
  - Every interaction is a "bunch crossing", where we have numerous "soft scatters" (elastic collisions), order 20 per crossing, which we want to ignore, and an occasionally "hard scatter" (inelastic collision), order 1 per collision, which we intend to select
- We refer to the location of a "hard scatter" as the Interaction Point (IP)
- We do not have knowledge of the spin state of the interacting protons, thus we often have to marginalize over spins producing a rate suppression for spin-dependent operators

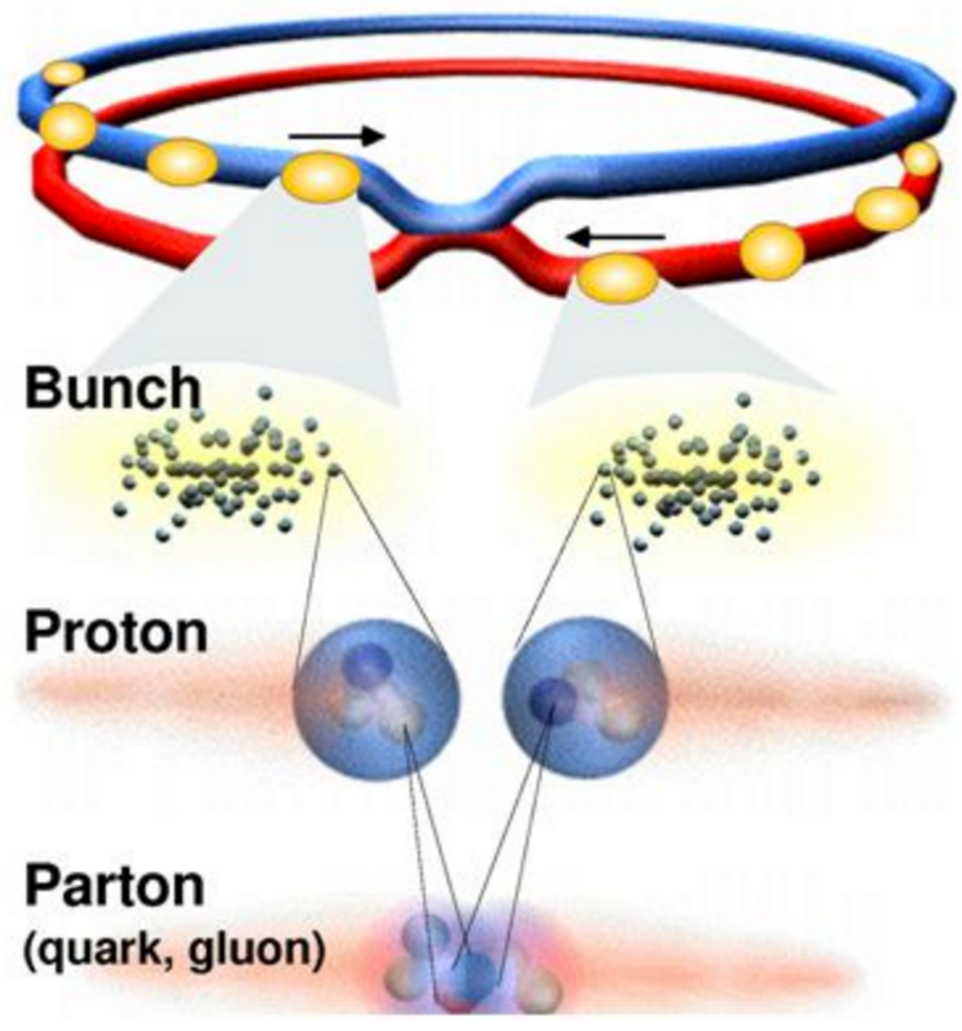

Figure from Andrew Beddall, TR-ATLAS Gaziantep Grid Workshop, June 19-21 2008

Standard Model Detector Signatures: Parton Model

- We can model the overall energy density of a hadron by imagining it as a tangle of partons (particles with non-neutral color charge)
  - Each parton has a relative size based on its interaction cross-section and energy density contribution
- Because the majority of the energy density of the nucleons is in gluon mediators, we have a probability of a loop diagram producing q/qbar pairs which mediate nucleon interactions
- Operators with anti-quarks and gluons are available to pp colliders due to the effective "parton distribution function" (PDF)

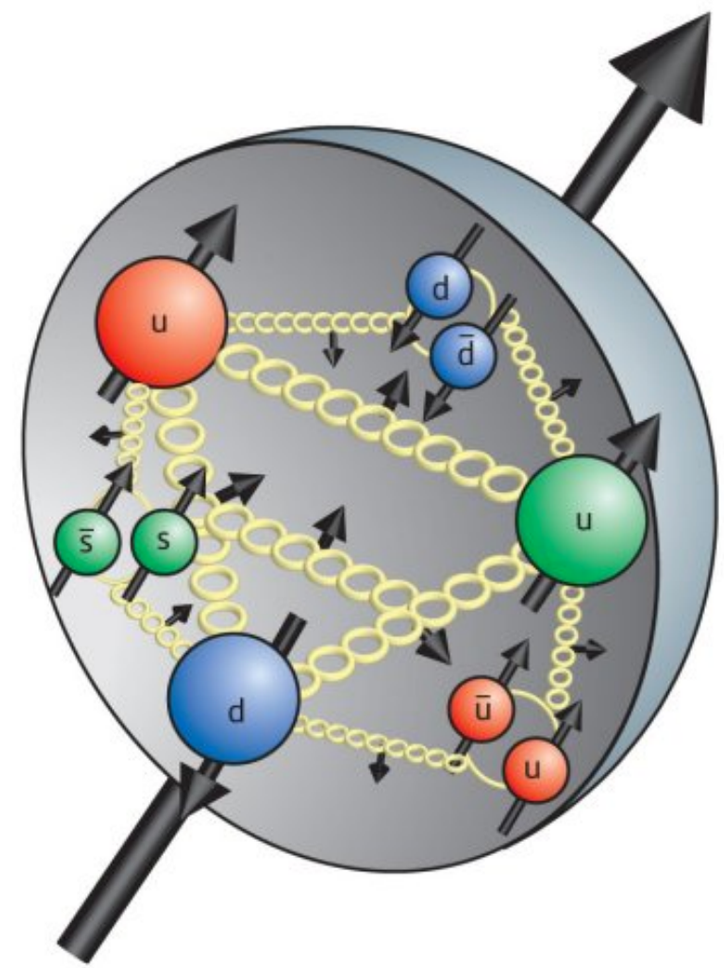

Proton in the Parton Model

Figures from quantumdiaries.org/2016/02/01/spun-out-of-proportion-the-proton-spin-crisis/

Standard Model Detector Signatures: Parton Model

- The form of the PDF is can be though of in a similar manner to nuclear form factors; it is a purely probabilistic description of the effective contribution of anti-quarks to the proton energy density
- We can draw diagrams with q/qbar initial states by multiplying the proton luminosity by the PDF probability for the input particles, and thus remove the protons from the rest of the modeling process
- We need to remember that the pardons came from nuclei, and be careful to remove remaining meson byproducts from the reconstruction

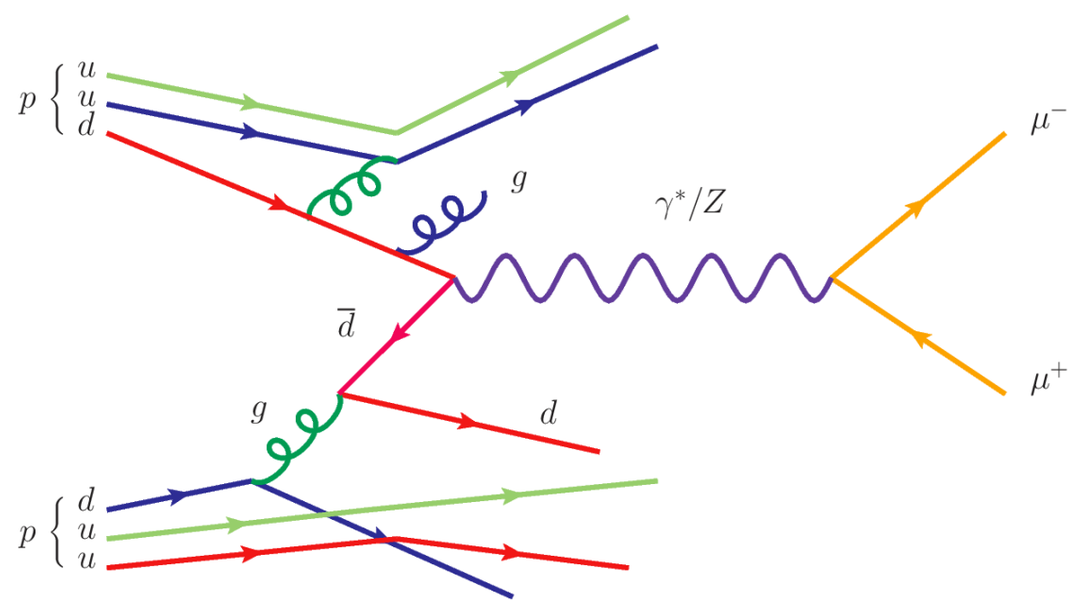

Figures from quantumdiaries.org/2016/02/01/spun-out-of-proportion-the-proton-spin-crisis/

Standard Model Detector Signatures: Final States

- Leptons - produce tracks, which differ greatly between flavor, curving according to charge to mass ratio and momentum
  - electrons produce charge showers
  - muons pass through the detector
- Photons - leave energy deposits in EM calorimeter, travel in straight lines
- Hadrons - stopped in the hadronic calorimeter, and are tagged as charged or uncharged based on track curvature
- Jets - hadron showers, clustered in conical shape about energetic axis
- Missing Transverse Energy (MEt) - after reconstruction, we infer the presence on non-interacting particles (neutrinos, WIMPs) by momentum conservation

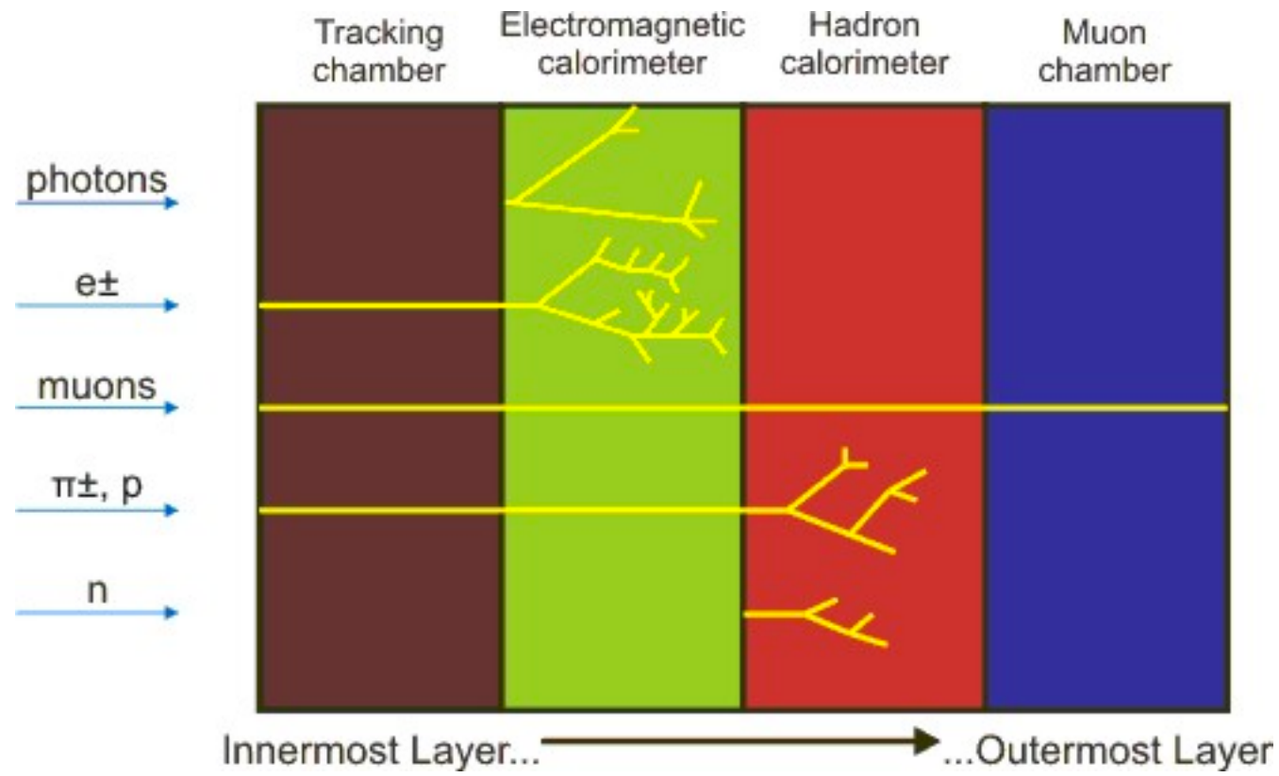

Image from http://hypatia.iasa.gr/en/help.html

Standard Model Detector Signatures: Decays

- Most particles decay near the IP, and don't make it to any of the detector layers; their existence is thus reconstructed from final states
  - All feynman diagrams for collider processes start at the quark/gluon level and end in detector final states

- Partons have to "hadronize" due to confinement and thus produce showers of particles called "jets" which leave tracks in all but the muon calorimeter

- Jets are very complicated objects, due to the non-perturbative nature of QCD
  - Charge usually uncertain
  - Defined by momentum parallel to a certain axis (jet axis) and include all particles within a certain radius
  - Easily corrupted by "pileup", particles produced in soft interactions that lie within jet cone

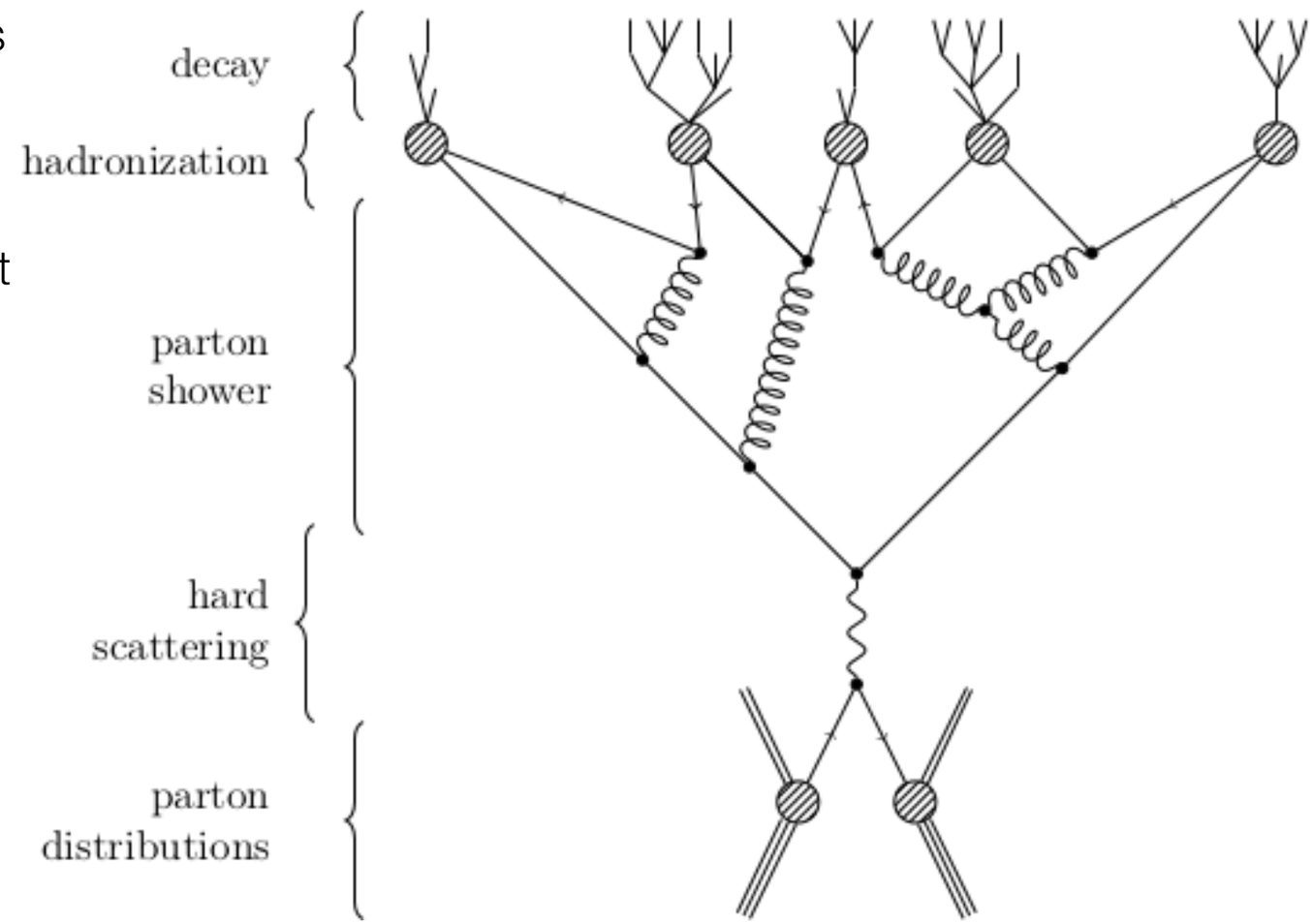

Standard Model Detector Signatures: Decays

- Most particles decay near the IP, and don't make it to any of the detector layers; their existence is thus reconstructed from final states
  - All feynman diagrams for collider processes start at the quark/gluon level and end in detector final states
- Partons have to "hadronize" due to confinement and thus produce showers of particles called "jets" which leave tracks in all but the muon calorimeter
- Jets are very complicated objects, due to the non-perturbative nature of QCD
  - Charge usually uncertain
  - Defined by momentum parallel to a certain axis (jet axis) and include all particles within a certain radius
  - Easily corrupted by "pileup", particles produced in soft interactions that lie within jet cone

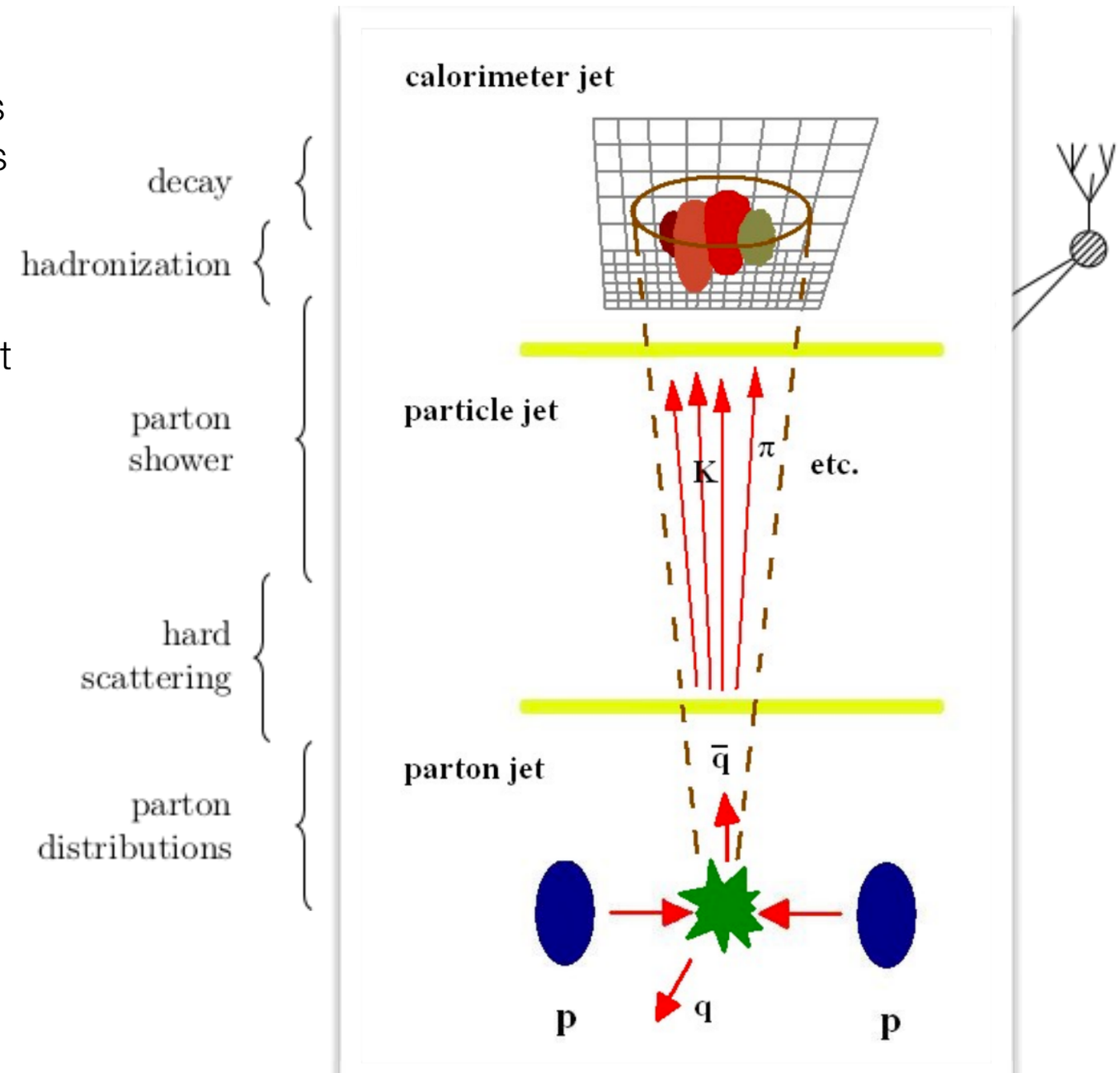

Modeling Dark Matter Production

- We assume WIMPs created via new mediator particle, which must be more massive than those produced at the LHC (otherwise we would have seen it as a distinct particle)

- For most massive mediators, this is a contact interaction, as the propagator in the limit of mass much greater than momentum becomes

$$\frac{ig_{\mu\nu}}{p^2 - m_{Z'}^2} \rightarrow \frac{-ig_{\mu\nu}}{m_{Z'}^2}$$

- In this limit we can model it effectively as a contact interaction, similar to the four-fermi theory for the weak interaction in the low energy limit, and develop an effective field theory

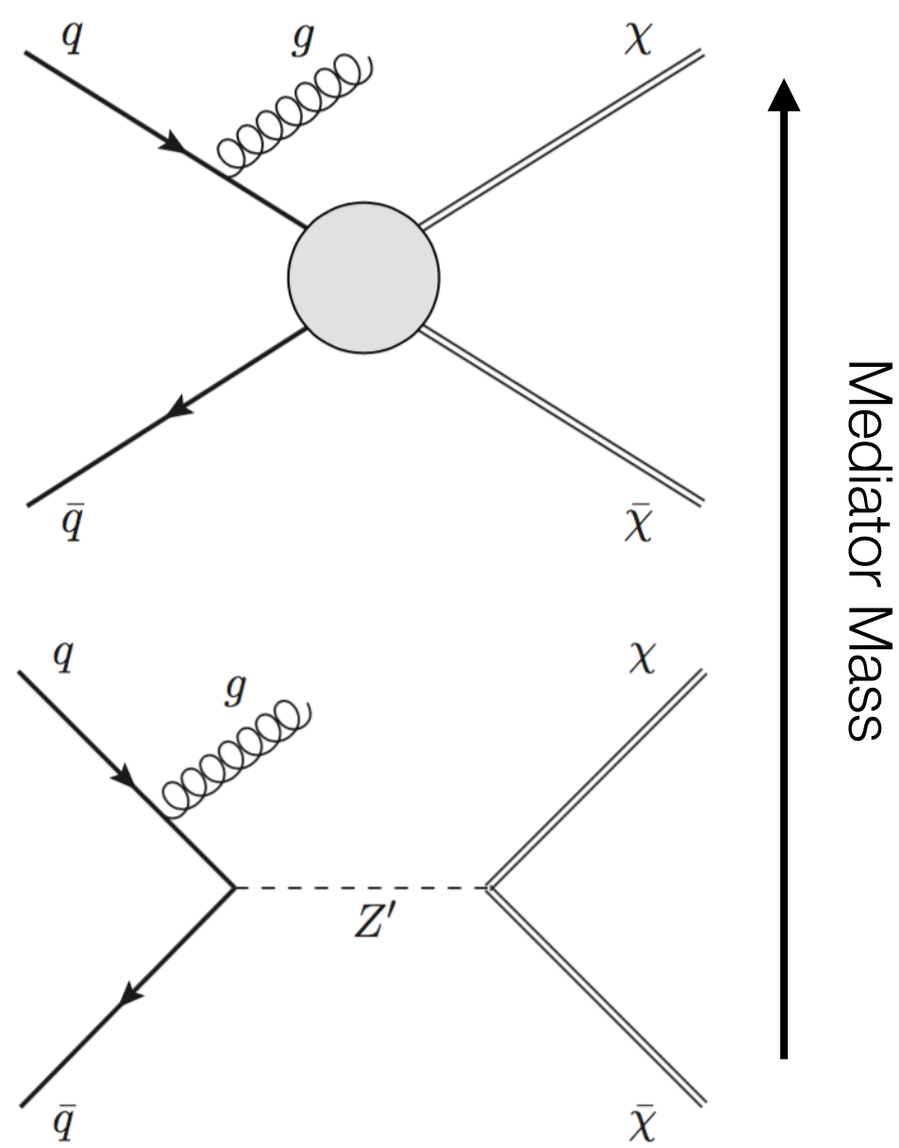

Figure adapted from Ref. 1 (ATLAS Collaboration 2014)

Dark Matter Collider EFT

- DM can be either scalar or Dirac fermion, which includes Majorana as special case
- (1) chose the operators shown at right from the complete EFT of (2), as they represent the six distinct spectral shapes for missing energy signal
- This is the subset of operators you get if you assume, to first order, no knowledge of spin states of either quarks or WIMPs
  - D8 is an exception, as it belongs to the same class as D5 but is used to convert collider limits into pair-production cross-sections for comparison to indirect searches

Name	Initial state	Type	Operator
C1	qq	scalar	$\frac{m_q}{M_\star^2}\chi^\dagger\chi\bar{q}q$
C5	gg	scalar	$\frac{1}{4M_\star^2}\chi^\dagger\chi\alpha_s(G^a_{\mu\nu})^2$
D1	qq	scalar	$\frac{m_q}{M_\star^3}\bar{\chi}\chi\bar{q}q$
D5	qq	vector	$\frac{1}{M_\star^2}\bar{\chi}\gamma^\mu\chi\bar{q}\gamma_\mu q$
D8	qq	axial-vector	$\frac{1}{M_\star^2}\bar{\chi}\gamma^\mu\gamma^5\chi\bar{q}\gamma_\mu\gamma^5 q$
D9	qq	tensor	$\frac{1}{M_\star^2}\bar{\chi}\sigma^{\mu\nu}\chi\bar{q}\sigma_{\mu\nu}q$
D11	gg	scalar	$\frac{1}{4M_\star^3}\bar{\chi}\chi\alpha_s(G^a_{\mu\nu})^2$

Table from Ref. 1 (ATLAS Collaboration 2014)

Simplified Massive Mediator Model

- Additionally, we can consider the very simple model of a single real massive mediator for mass near the momentum transfer scale, where we have the Dirac WIMP interaction Lagrangian

$$\mathcal{L}_{int} = Z'(g_q q\bar{q} + g_\chi \chi\bar{\chi})$$

- This gives the matrix element conversion

$$\mathcal{M} \propto \frac{g_q g_\chi}{M_{med}^2} = \frac{1}{M_Z^2} \rightarrow M_{med} = \sqrt{g_q g_\chi} M_Z$$

- So we have a free parameter, the coupling product, which allows us to explore the effect of the mediator mass in the pure EFT, and constrain the product of quark and WIMP couplings

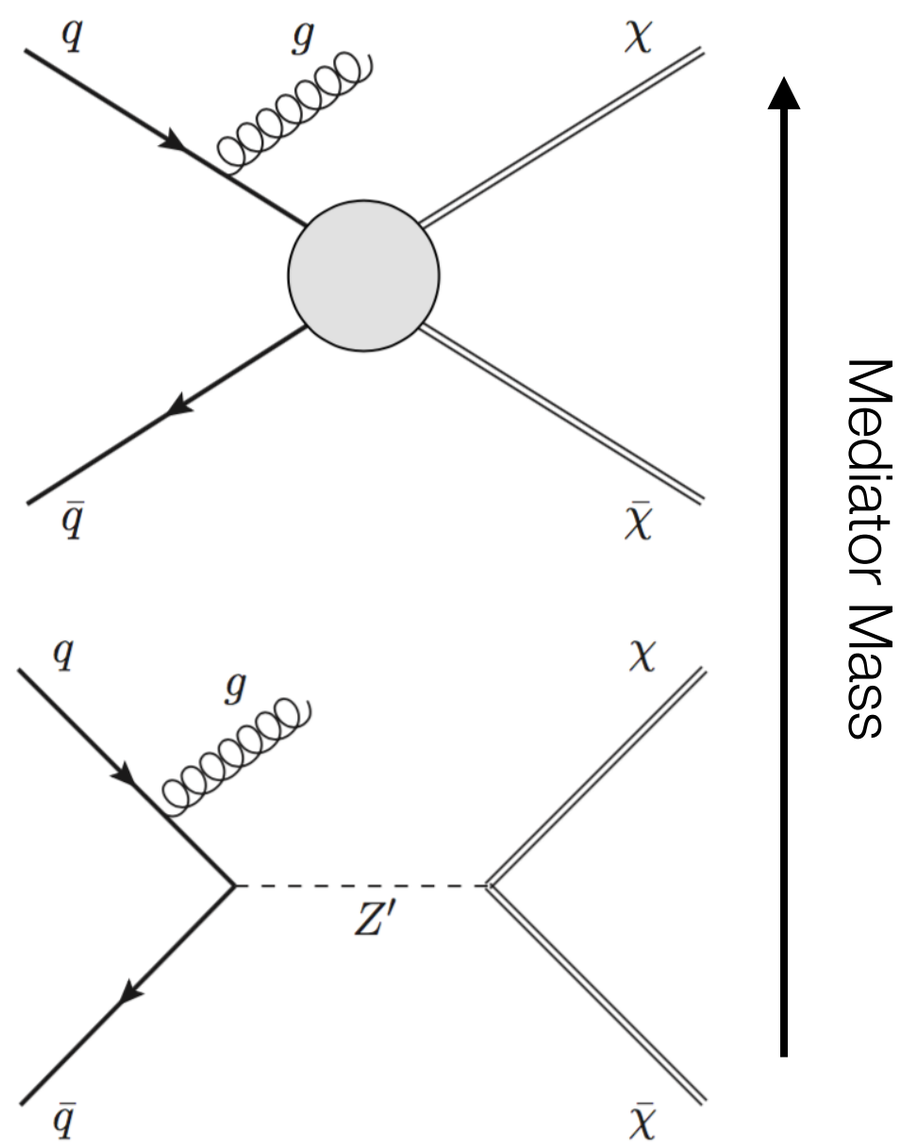

Figure adapted from Ref. 1 (ATLAS Collaboration 2014)

Simplified Massive Mediator Model

Operator(s)	Relation between M_{med} and $M_\star$	Coupling term range
D1	$M_{\text{med}} = \sqrt{y_q g_\chi}\ \sqrt{M_\star^3/m_q}$	$0 < \sqrt{y_q g_\chi} < 4\pi$
C1	$M_{\text{med}} = y_q \lambda_\chi \zeta_\lambda\ M_\star^2/m_q$	$0 < y_q \lambda_\chi \zeta_\lambda < (4\pi)^2 \zeta_\lambda$
D5, D8, D9	$M_{\text{med}} = \sqrt{g_q g_\chi}\ M_\star$	$0 < \sqrt{g_q g_\chi} < 4\pi$
D11	$M_{\text{med}} = \sqrt[3]{a g_\chi}\ M_\star$	$0 < \sqrt[3]{a g_\chi} < \sqrt[3]{16\pi}$
C5	$M_{\text{med}} = \sqrt{a \lambda_\chi \zeta_\lambda}\ M_\star$	$0 < \sqrt{a \lambda_\chi \zeta_\lambda} < 4\sqrt{\pi \zeta_\lambda}$

- This procedure is modified slightly for the operators which have different coupling forms
  - In D1 and C1, it is assumed to be a Yukawa coupling, and we also need to account for the addition quark mass term in our EFT coefficient
  - D11 and C5 explicitly take into account the loop diagram discussed in the quark coupling slide

- For the theory to remain perturbative, we need the coupling to remain in the given range, where normal couplings are less than 4*pi, and a<4.

- These relations are used to explore deviations from the pure EFT framework by perturbing the EFT about its natural scale. For this model, limits are only expressed for momentum transfer below the mediator mass for a given coupling, where a smaller coupling will thus impose a more restrictive limit

Quark Interactions: Standard Model Background

- The first feature of these operators we notice is that the tree-level diagrams are in principle unobservable:

$$pp\ (p\bar{p}) \to X\bar{X}$$

- We require some initial state radiation (ISR), as shown in the diagram at the top right and represented by the process, to tag potential events through missing traverse momentum:

$$pp\ (p\bar{p}) \to X\bar{X} + \text{jets}$$

- This opens up the analysis to standard model backgrounds which produce a single jet + mEt, as well as processes with leptons missed in reconstruction:

$$pp\ (p\bar{p}) \to \nu\bar{\nu} + \text{jets}$$
$$pp\ (p\bar{p}) \to l^-\bar{\nu} + \text{jets}$$
$$pp \to t\bar{t} \to W^+b\ W^-\bar{b},$$

- Suppression in quarks comes from PDF and ISR vertex, otherwise these are tree-level diagrams
  - Spin dependent operators are additionally suppressed due to integration twice over initial spin state

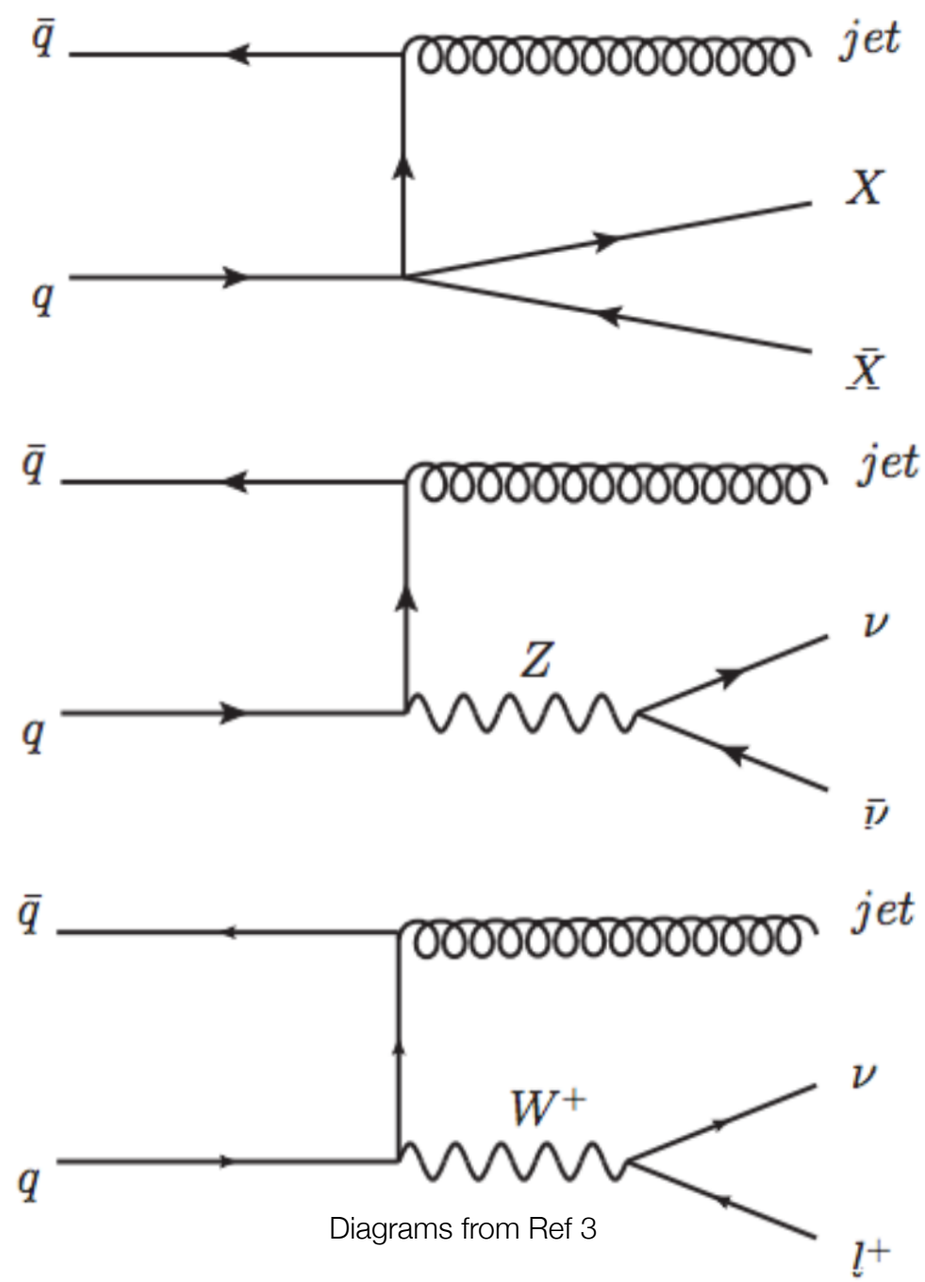

Diagrams from Ref 3

Gluon Interactions

- Gluons also contribute due to their PDF contribution, with integration over color charges and slight suppression from the ISR
- The EFT couplings have a strong force suppression from the gluon-fusion process, so the gluon couplings are likely (virtual) quark couplings
- This is also implicitly a sum over a large number of quark operators, so it still represents a distinct spectral shape
- In addition the overall rate calculation is different, as these are gluons, not quark/antiquark pairs, in the initial state, so amount of available phase space will be different

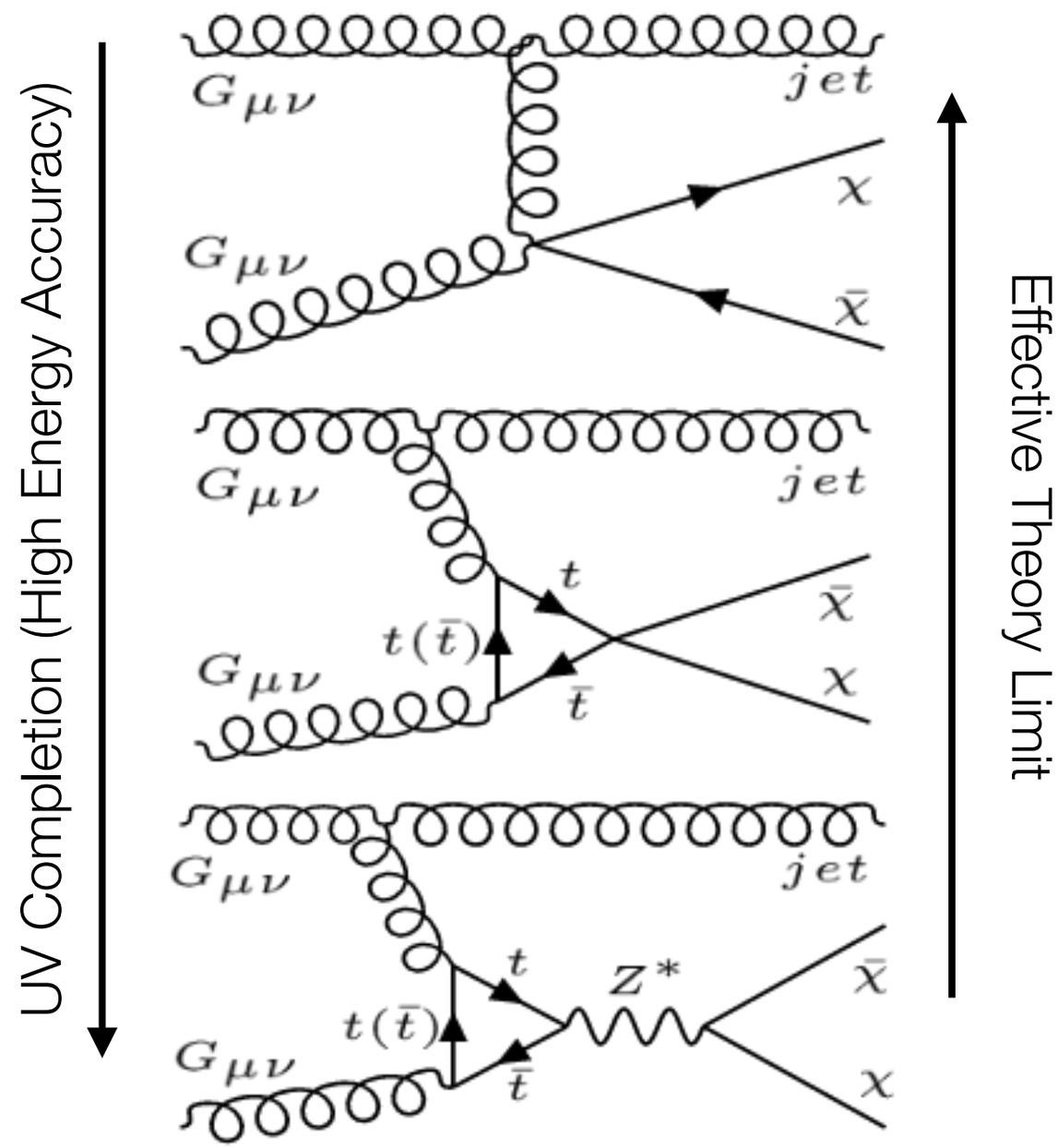

Collider to Scattering Cross-Section Conversion

- The EFT and massive mediator models can be converted to scattering cross-sections parameterized in WIMP mass, WIMP-nucleon reduced mass, and suppression scale in the low momentum transfer limit
- Dirac WIMPs - constraints become tighter with reduced WIMP mass for a given mediator mass
- Scalar WIMPs - trends are flat until reduced WIMP mass becomes proton mass, weaker thereafter
- Spin-dependent interactions (D1, D11) have much stronger dependence on suppression scale, and can be expected to be tighter

$$\sigma_0^{\mathrm{D1}} = 1.60 \times 10^{-37}\ \mathrm{cm}^2 \left(\frac{\mu_\chi}{1\ \mathrm{GeV}}\right)^2 \left(\frac{20\ \mathrm{GeV}}{M_*}\right)^6,$$

$$\sigma_0^{\mathrm{D5,C3}} = 1.38 \times 10^{-37}\ \mathrm{cm}^2 \left(\frac{\mu_\chi}{1\ \mathrm{GeV}}\right)^2 \left(\frac{300\ \mathrm{GeV}}{M_*}\right)^4,$$

$$\sigma_0^{\mathrm{D8,D9}} = 9.18 \times 10^{-40}\ \mathrm{cm}^2 \left(\frac{\mu_\chi}{1\ \mathrm{GeV}}\right)^2 \left(\frac{300\ \mathrm{GeV}}{M_*}\right)^4,$$

$$\sigma_0^{\mathrm{D11}} = 3.83 \times 10^{-41}\ \mathrm{cm}^2 \left(\frac{\mu_\chi}{1\ \mathrm{GeV}}\right)^2 \left(\frac{100\ \mathrm{GeV}}{M_*}\right)^6,$$

$$\sigma_0^{\mathrm{C1,R1}} = 2.56 \times 10^{-36}\ \mathrm{cm}^2 \times \left(\frac{\mu_\chi}{1\ \mathrm{GeV}}\right)^2 \left(\frac{10\ \mathrm{GeV}}{m_\chi}\right)^2 \left(\frac{10\ \mathrm{GeV}}{M_*}\right)^4,$$

$$\sigma_0^{\mathrm{C5,R3}} = 7.40 \times 10^{-39}\ \mathrm{cm}^2 \times \left(\frac{\mu_\chi}{1\ \mathrm{GeV}}\right)^2 \left(\frac{10\ \mathrm{GeV}}{m_\chi}\right)^2 \left(\frac{60\ \mathrm{GeV}}{M_*}\right)^4,$$

Equations from Ref. 2 (Goodman et. al. 2010)

- Experimental Setup
  - The ATLAS Detector and Event Reconstruction
  - BSM Physics in the Monojet Channel
  - Expected backgrounds
  - Signal and Background Simulations

Some Experimental Particle Physics Terminology

- Soft and hard scatters need to be distinguished; soft-scatters do not transfer a large amount of momentum, and thus will have low momentum perpendicular to the beam axis.

- We can define quantities relative to the normal to the beam axis which will allow us to separate hard and soft-scatter interactions. Pseudorapidity (η) represents the fraction of a particle's longitudinal to total momentum:

$$\eta = -\ln\left[\tan\left(\frac{\theta}{2}\right)\right] = \tanh^{-1}\left(\frac{p_L}{|p|}\right)$$

- We also measure transverse momentum pT, which relates to total particle momentum as

$$|p| = p_T \cosh(\eta)$$

- The sum of transverse momentum gives us, to first order, the amount of momentum transfer from a scatter process, as the initial state is constructed such that the sum of transverse momentum is 0. By making a pT cut, we can select increasingly energetic reactions.

The ATLAS Detector

- The ATLAS detector consists of layers of detectors similar to those shown earlier which allow for identification of particles based on energy and charge-to-mass ratio

- We want to make sure all particles from the event had a chance to interact with all layers, for full event reconstruction
  - Different layers will have different coverage in pseudorapidity

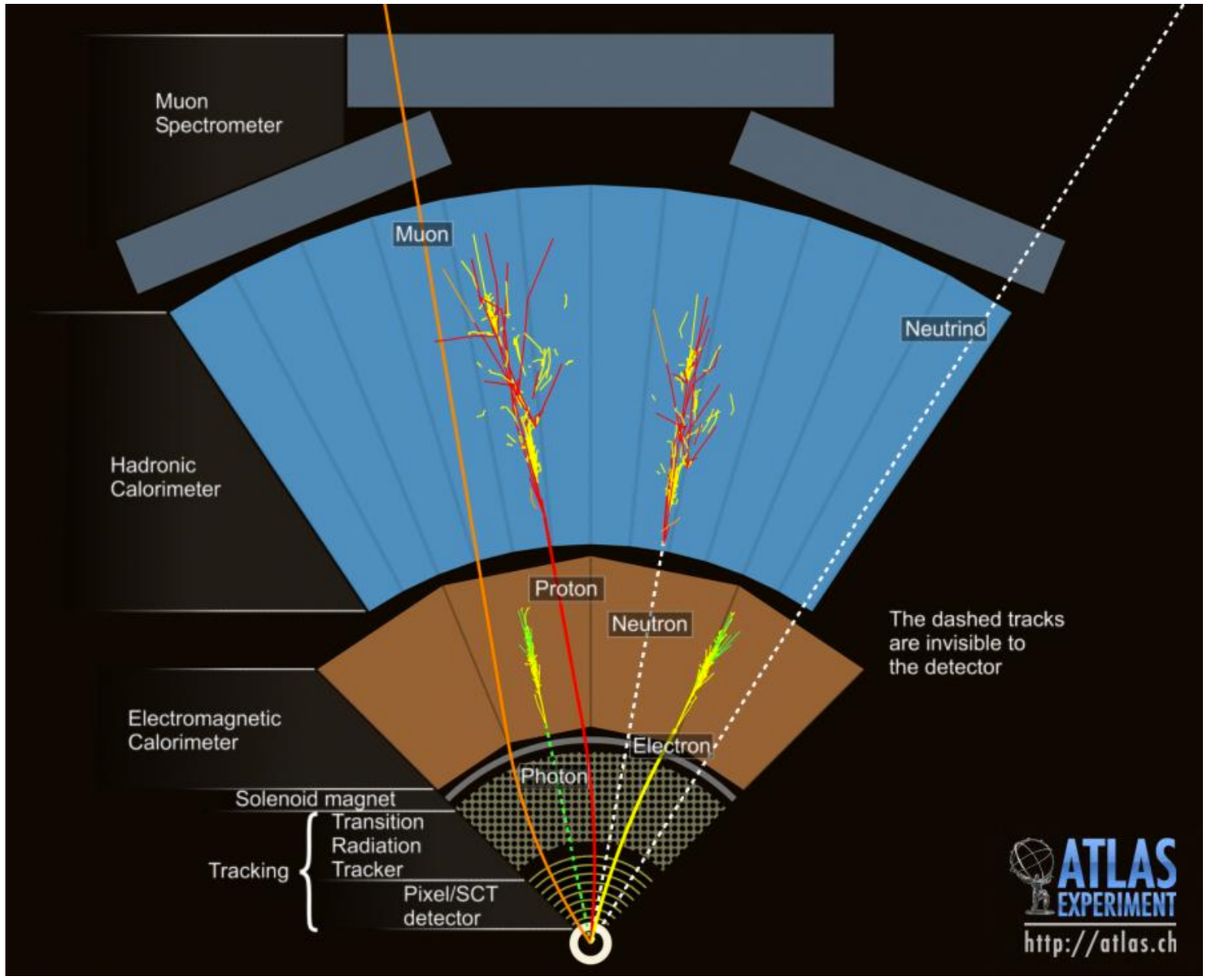

The ATLAS Detector: Angular Coverage

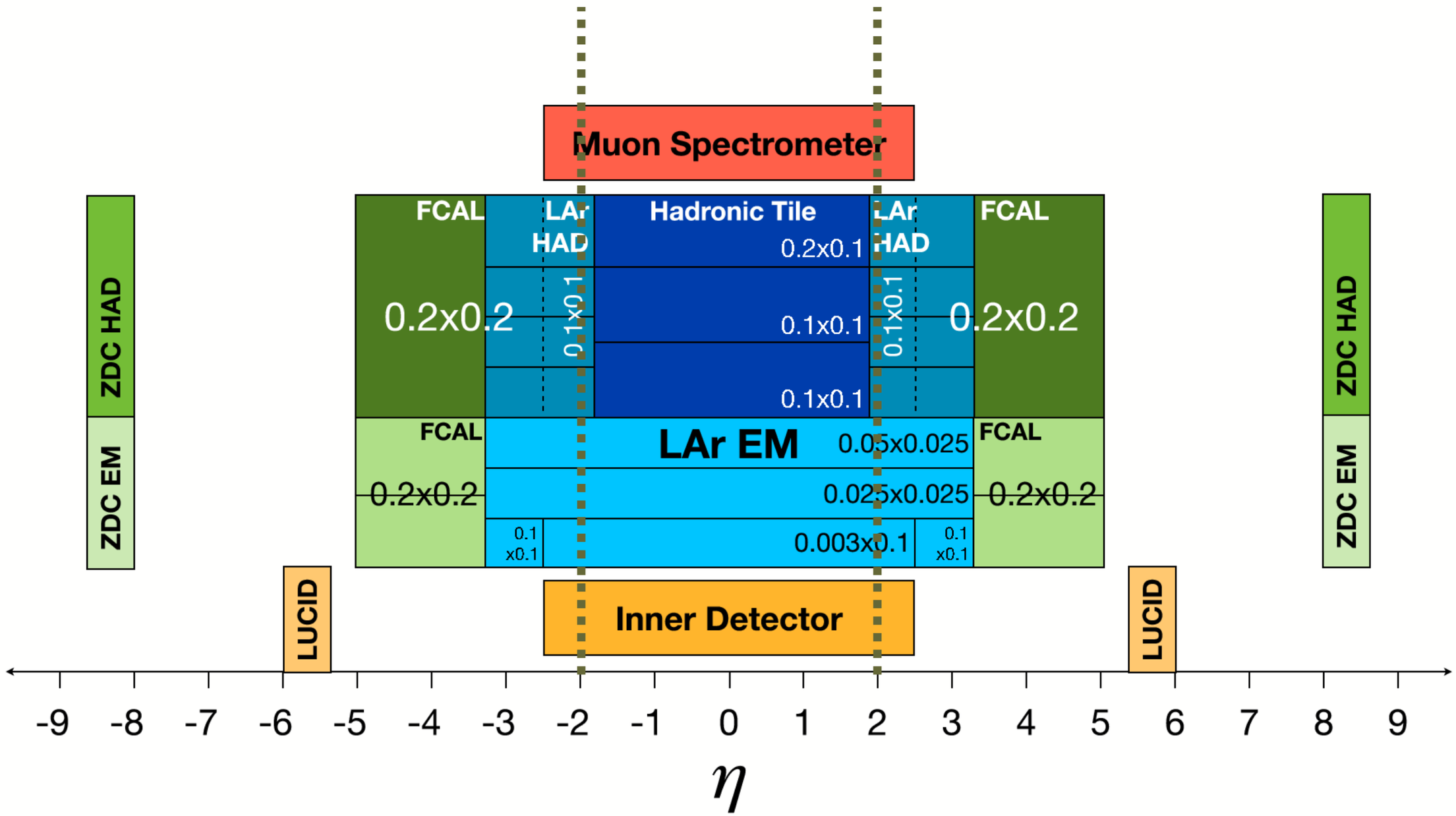

Event Reconstruction

- Jets are constructed from calorimeter deposits by a jet clustering algorithm, and required to be within a radius of 0.4 radians

- Reducible backgrounds have leptons in the final states
  - Need to select events where tracks can be identified as leptons with high confidence
  - Should reject jets which are roughly co-linear with tagged leptons, as these are most likely mis-reconstructed

- Final monojet signal should reject events with any lepton final states, but lepton final states should be used to validate Monte Carlo simulations of irreducible background

- Missing energy constructed by considering all energy deposits in the calorimeter away from boundaries, and missing transverse momentum reconstructed from the resulting net transverse momentum

Event Selection

Table 2 Event selection criteria applied for the selection of monojet-like signal regions, SR1–SR9.

Selection criteria									
Preselection									
Primary vertex									
$E_{\mathrm{T}}^{\mathrm{miss}} > 150$ GeV									
Jet quality requirements									
At least one jet with $p_{\mathrm{T}} > 30$ GeV and $\lvert\eta\rvert < 4.5$									
Lepton and isolated track vetoes									
Monojet-like selection									
The leading jet with $p_{\mathrm{T}} > 120$ GeV and $\lvert\eta\rvert < 2.0$									
Leading jet $p_{\mathrm{T}}/E_{\mathrm{T}}^{\mathrm{miss}} > 0.5$									
$\Delta\phi(\mathrm{jet}, \mathbf{p}_{\mathrm{T}}^{\mathrm{miss}}) > 1.0$									
Signal region	SR1	SR2	SR3	SR4	SR5	SR6	SR7	SR8	SR9
Minimum $E_{\mathrm{T}}^{\mathrm{miss}}$ [GeV]	150	200	250	300	350	400	500	600	700

- Final monojet-like events required to have jet passing through pseudorapidity range of all detector layers
- Jet criteria prevent signal excess from mis-reconstructed jets
  - Leading jet must balance a substantial fraction of the missing energy
  - Jet and missing pT must have appreciable angular separation
- Signal regions represent increasingly strict missing energy criteria, which will have both reduced backgrounds and reduce signal; the region with the highest signal to noise will be chosen for each operator

Backgrounds Considered

- As shown earlier, the two leading backgrounds will be the electroweak backgrounds

$$Z \to \nu\bar{\nu} + jets$$
$$W^+ \to l^+\nu + jets$$
$$W^- \to l^-\bar{\nu} + jets$$

- In addition, we can imagine remaining backgrounds leaking in due to limited tracking/tagging efficiency, including diboson events as well as

$$Z/\gamma^* \to l\bar{l} + jets$$
$$t\bar{t} \to b\bar{b} + jets$$
$$t\bar{t} \to b\bar{b} + l\nu + jets$$
$$t \to b\bar{b} + l\nu$$

- Finally, there are data driven backgrounds such as jet reconstruction error (multijet background) and non-collision background from beam fluctuations

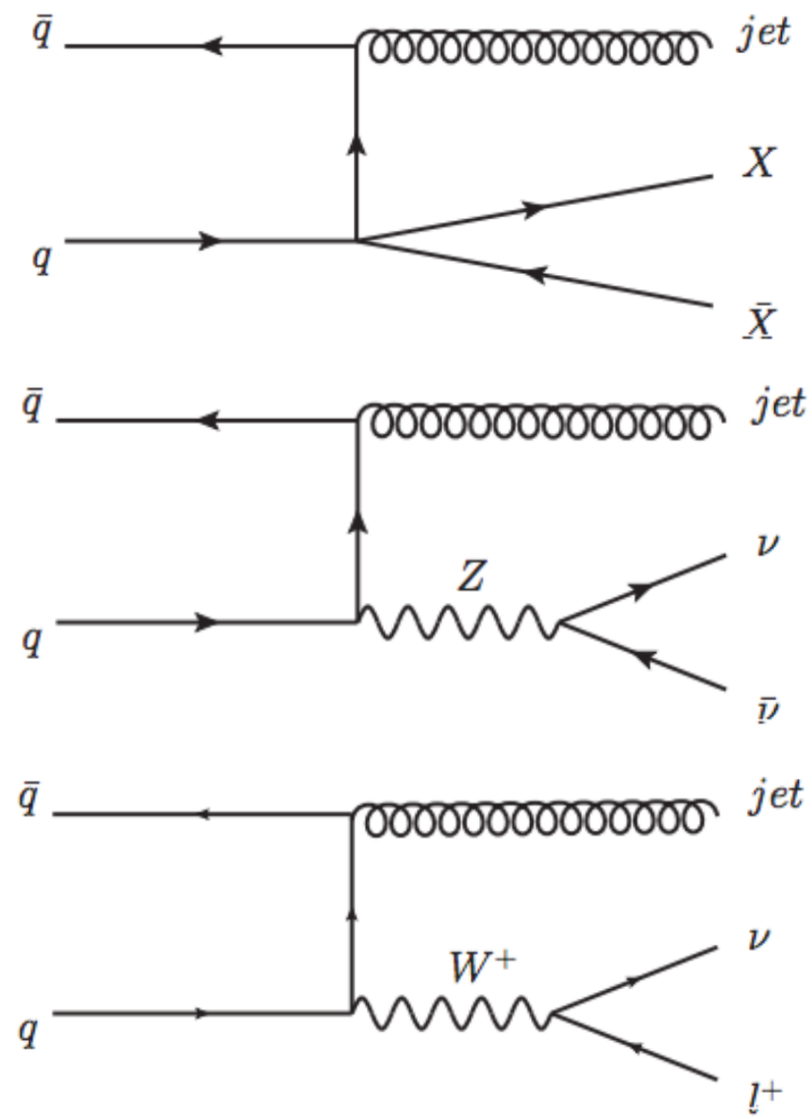

Background and Signal Simulation

Table 3 Summary of the methods and control samples used to constrain the different background contributions in the signal regions.

Background process	Method	Control sample
$Z(\to \nu\bar{\nu})$+jets	MC and control samples in data	$Z/\gamma^*(\to \ell^+\ell^-)$, $W(\to \ell\nu)$ $(\ell = e, \mu)$
$W(\to e\nu)$+jets	MC and control samples in data	$W(\to e\nu)$ (loose)
$W(\to \tau\nu)$+jets	MC and control samples in data	$W(\to e\nu)$ (loose)
$W(\to \mu\nu)$+jets	MC and control samples in data	$W(\to \mu\nu)$
$Z/\gamma^*(\to \ell^+\ell^-)$+jets $(\ell = e, \mu, \tau)$	MC-only	
$t\bar{t}$, single top	MC-only	
Diboson	MC-only	
Multijets	data-driven	
Non-collision	data-driven	

- Standard ATLAS Monte Carlo codes are used to simulate each background assuming luminosity ~ 20 inverse femtobarns and CM energy of 8 TeV
  - Corresponds to a cross-section of 5e-41 producing 1 event
- Monte Carlo data sent through same selection as signal region, excluding muon and electron cuts
- Dominant processes re-scaled based on “control regions”, SR1 regions with muon veto coincidence, to reduce background uncertainties, collected by the Etmiss trigger
  - Electron backgrounds collected by employing data from a separate electron trigger and applying same jet and missing energy quality cuts

Background Validation from Control Regions

- The leading backgrounds are scaled from the control regions according to the equations

$$N_{\text{signal}}^{W(\to\mu\nu)} = \frac{(N_{W(\to\mu\nu),\text{control}}^{\text{data}} - N_{W(\to\mu\nu),\text{control}}^{\text{non}-W/Z})}{N_{W(\to\mu\nu),\text{control}}^{\text{MC}}} \times N_{\text{signal}}^{\text{MC}(W(\to\mu\nu))} \times \xi_\ell \times \xi_{\text{trg}} \times \xi_\ell^{\text{veto}}$$

$$N_{\text{signal}}^{Z(\to\nu\bar{\nu})} = \frac{(N_{W(\to\mu\nu),\text{control}}^{\text{data}} - N_{W(\to\mu\nu),\text{control}}^{\text{non}-W/Z})}{N_{W(\to\mu\nu),\text{control}}^{\text{MC}}} \times N_{\text{signal}}^{\text{MC}(Z(\to\nu\bar{\nu}))} \times \xi_\ell \times \xi_{\text{trg}},$$

- The efficiency terms come from potential trigger and veto rate differences between MC and data, which are expected to be within 1% of unity
- The correction factors here ranged from 0.9 to 0.6 as the missing energy threshold was increased
- The same scaling was done for electron backgrounds from the electron control samples
- This scaling thus effectively reduces background uncertainty from the 20-40% level closer to the 1-5% level, once all uncertainties are accounted for

Muon control regions

- Single muon region constrains charge decays
- W decay dominates the muon signal in most signal variables
- In low jet multiplicity (panel d), W sample dominates, but ttbar background dominates at high jet multiplicity
- At higher energy, we are statistics limited, but Diboson signal starts to have significant contribution

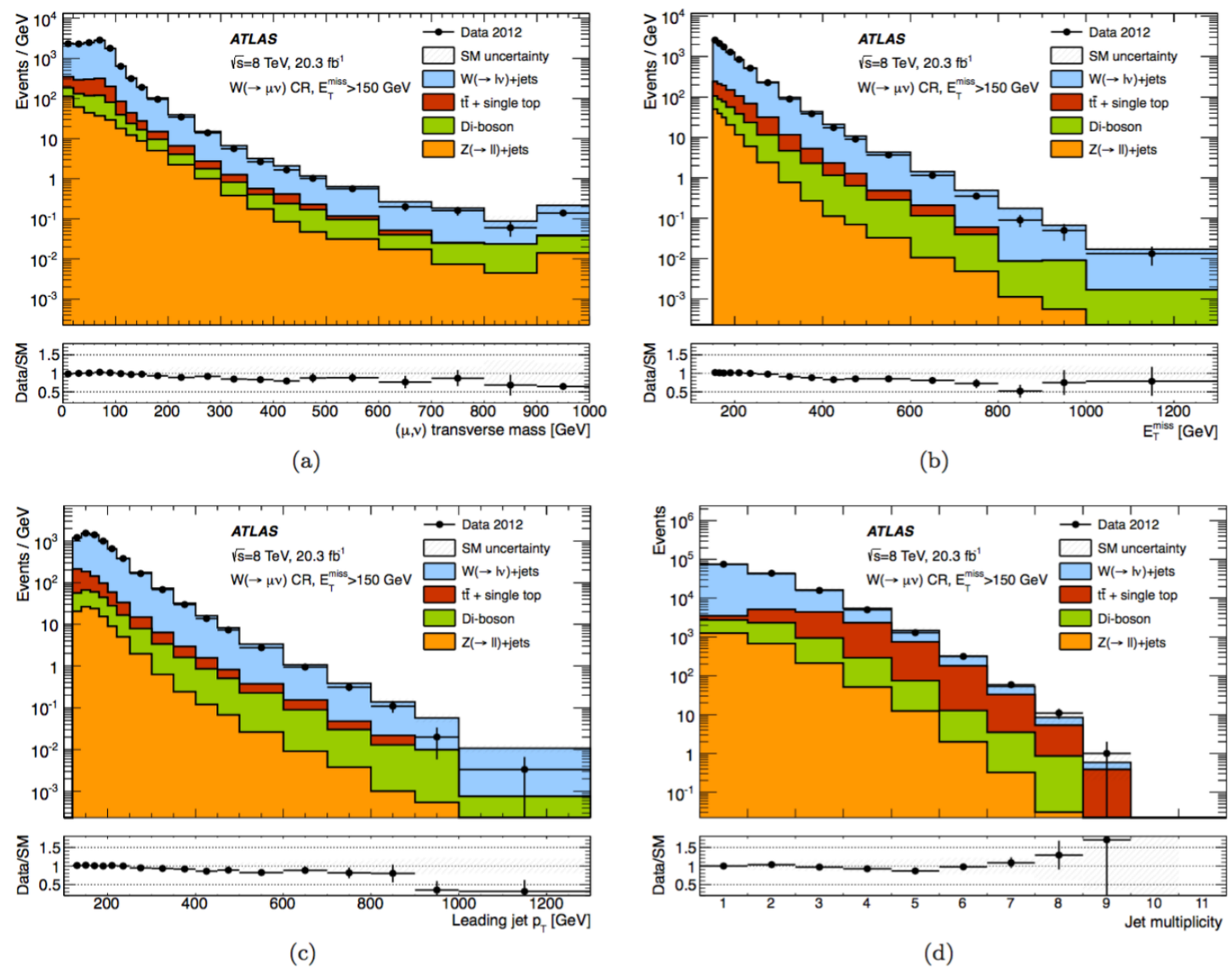

Fig. 2 Distributions of the measured (a) transverse mass of the identified muon and the missing transverse momentum, (b) $E_{\mathrm{T}}^{\mathrm{miss}}$, (c) leading jet p_{T} and (d) jet multiplicity distributions in the $W(\rightarrow \mu\nu)$+jets control region for the inclusive SR1 selection, compared to the background expectations. The latter include the global normalization factors extracted from the data. Where appropriate, the last bin of the distribution includes overflows. The lower panels represent the ratio of data to MC expectations. The error bands in the ratios include the statistical and experimental uncertainties on the background expectations.

Dimuon control regions

- Dimuon channel constrains neutral decays
- Z decay dominates the muon signal in most signal variables, closely followed by the Diboson signal
- W sample leaks in here as a mis-tagging of a jet as a charge; this combined with the previous region allows us to measure reconstruction efficiencies
- Missing energy signal has noise fall as a power law

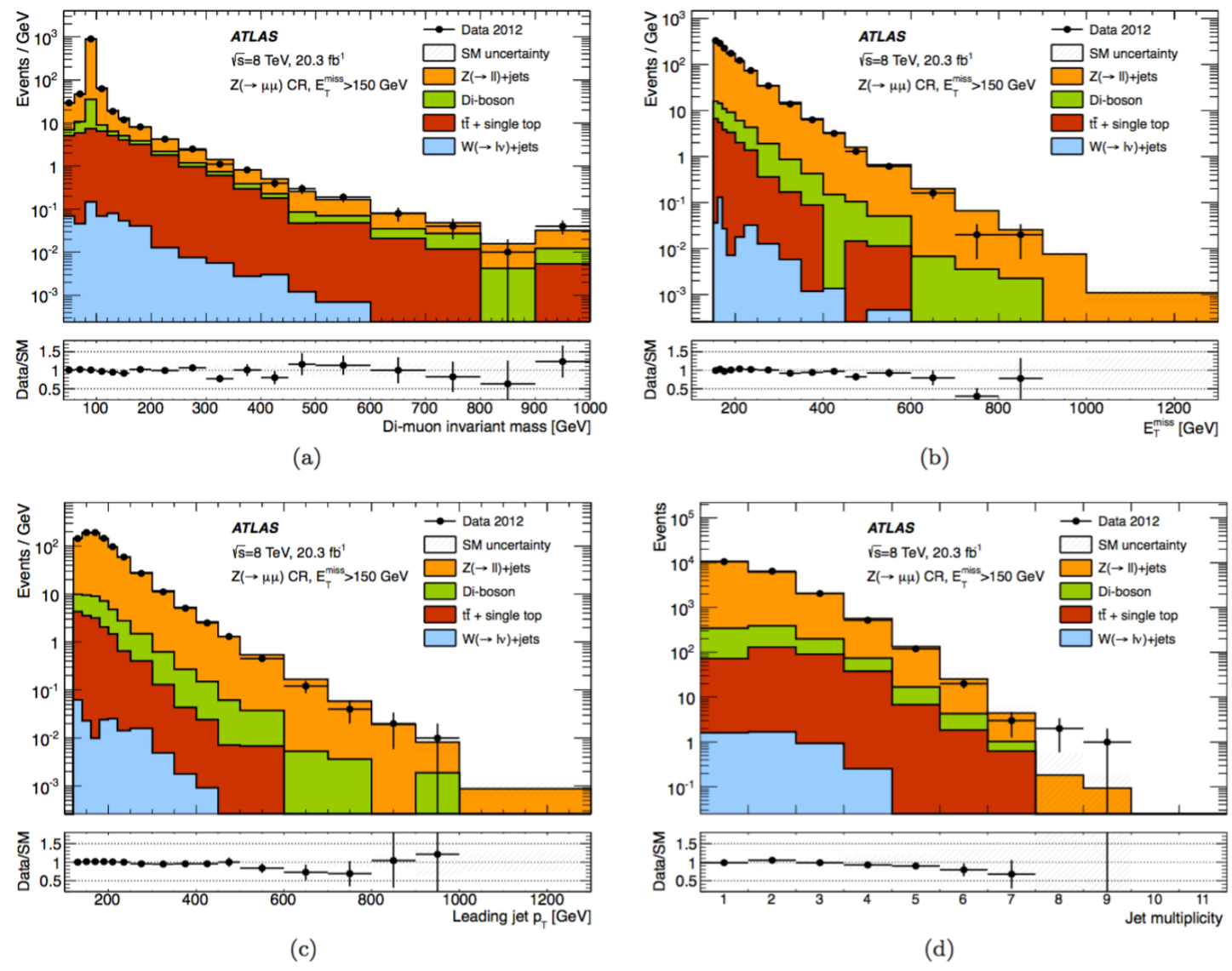

Fig. 3 Distributions of the measured (a) dilepton invariant mass, (b) $E_{\mathrm{T}}^{\mathrm{miss}}$, (c) leading jet p_{T} and (d) jet multiplicity distributions in the $Z/\gamma^*(\rightarrow \mu^+\mu^-)$+jets control region for the inclusive SR1 selection, compared to the background expectations. The latter include the global normalization factors extracted from the data. Where appropriate, the last bin of the distribution includes overflows. The lower panels represent the ratio of data to MC expectations. The error bands in the ratios include the statistical and experimental uncertainties on the background expectations.

Background Uncertainties

- Leading uncertainty contribution in experimental errors comes from uncertainty in the jet energy scale, and jet energy resolution (sys), which is at the 1-3% level
  - Mis-classification uncertainties are already accounted for through use of the MC data, and rescaling from control regions

- Some amount of uncertainty remains for the sub-dominant control processes in MC production
  - These contribute to the signal more in the regions of high energy threshold

- Due to the perturbative nature of some of the MC calculations, there is a controlled degree of approximation which contributes ~1-3% uncertainty

- Final uncertainty ranges from ~3% in SR1, to 6.2% for SR7, to 14% for SR9

- Results and Conclusions
  - Signal Measurement
  - Limits on mediator mass
  - Comparison to direct and indirect cross-section limits
  - Future Prospects (Run 2 and beyond)

Results: No Excesses in Any Signal Region (SR1)

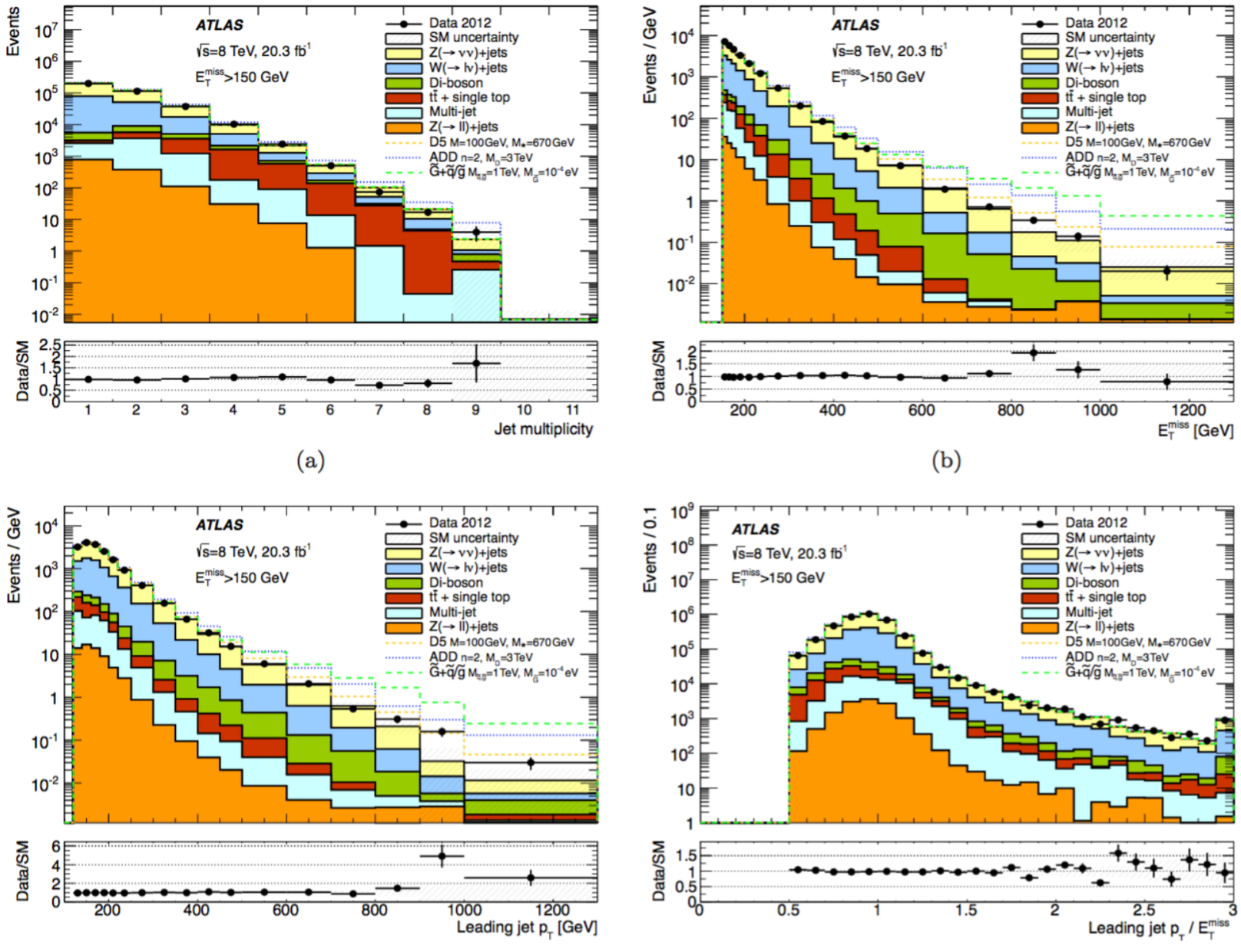

Results: No Excesses in Any Signal Region (HT)

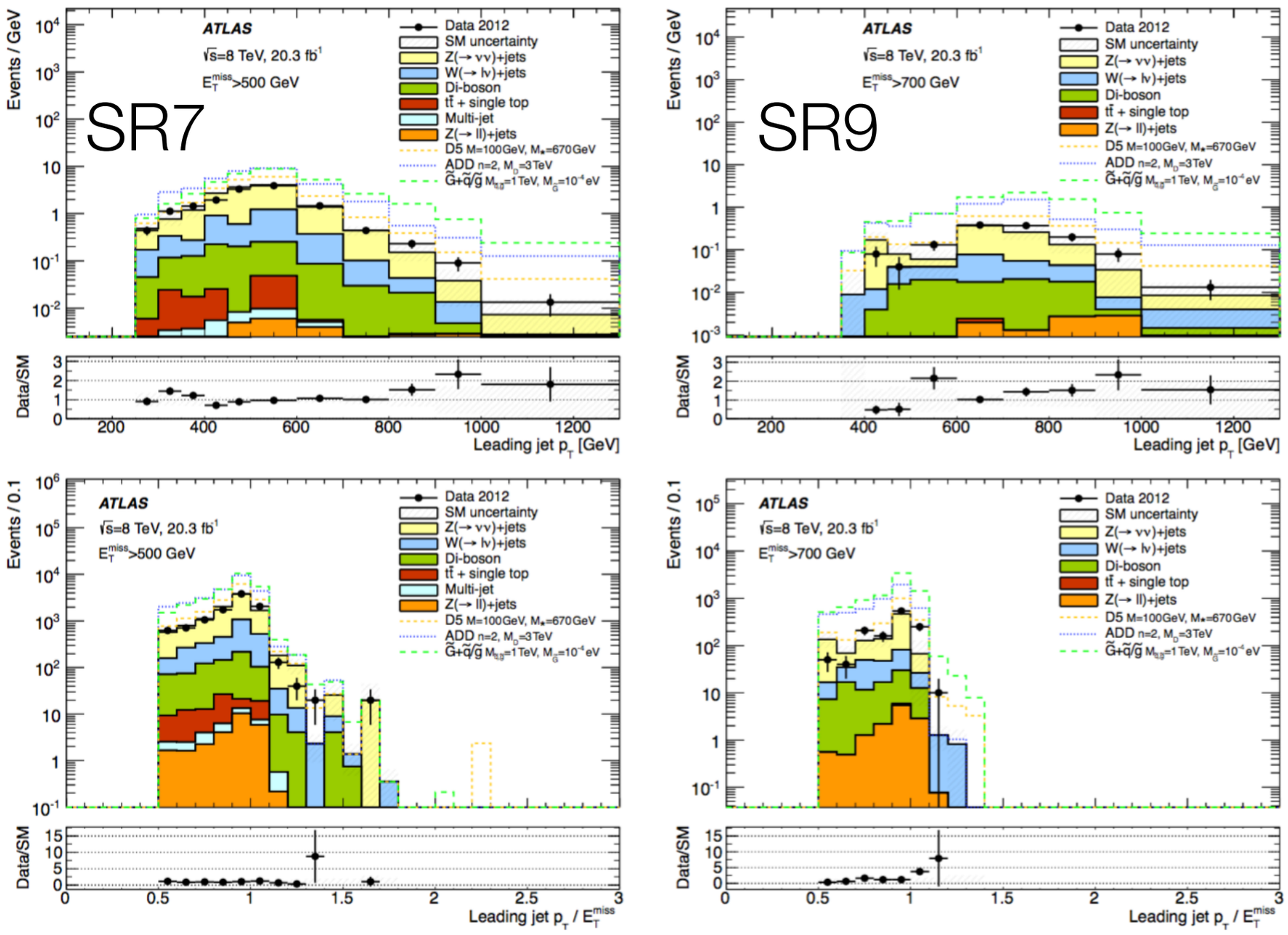

(a) (b)

Suppression Scale Limits: Quark Couplings

- Solid lines indicate correct mass/cross section for relic abundance
- Suppression scale for D1 is very low, constraints are not very strict
- D5-D9 are much more constrained, even in the truncated coupling limit (weak EFT limit)
- Correct relic abundance due to dark matter ruled out at low mass for all Dirac operators, but not at high mass, except for D8

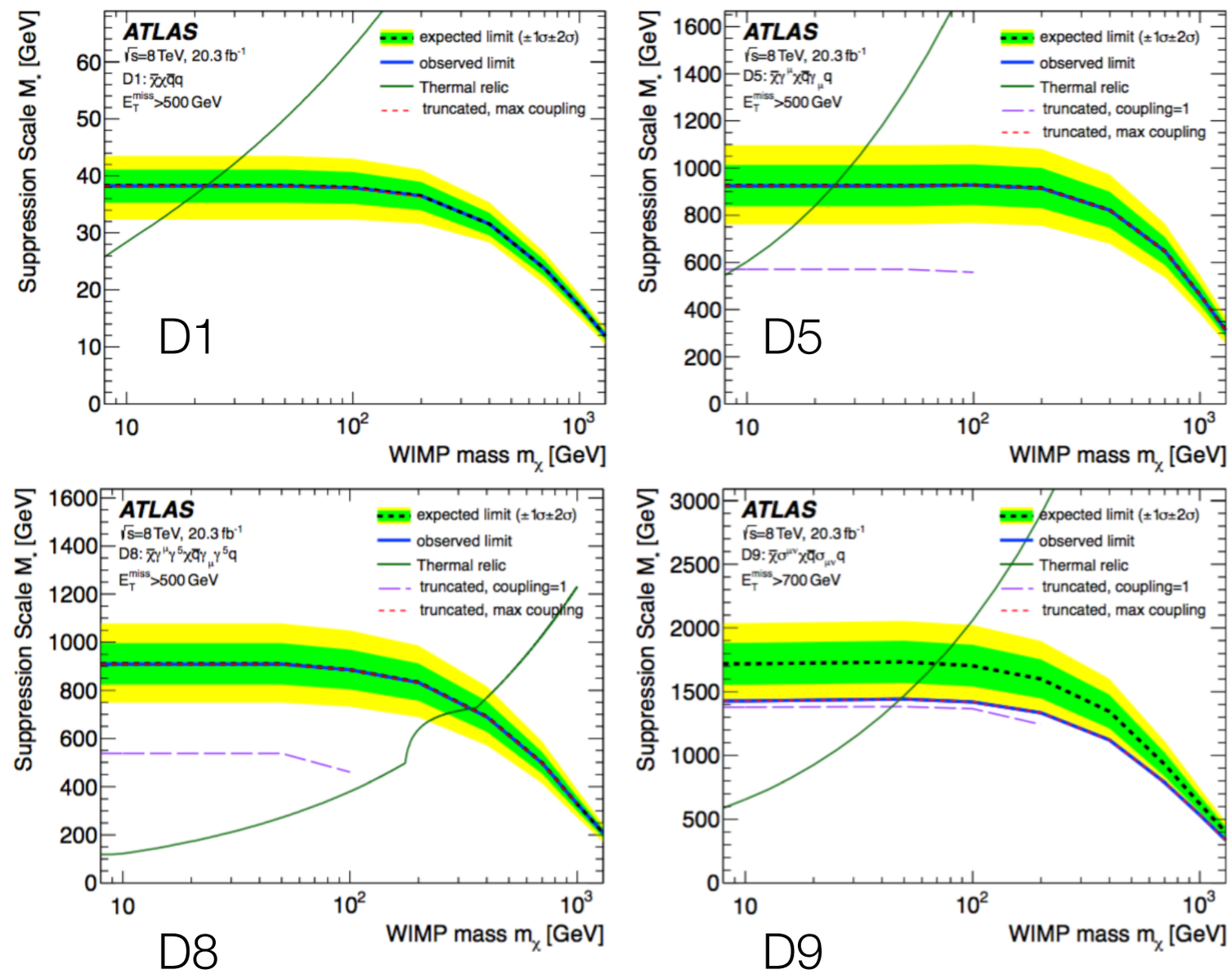

Suppression Scale Limits: Gluon Couplings

- Again, suppression scale limits are not as high as one might expect, and thermic relic abundance not ruled out
- All constraints should be valid for the lightest dark matter in most cases
- Relic abundance is clearly ruled out for Dirac spinor, but still allowed for range of complex scalar interactions

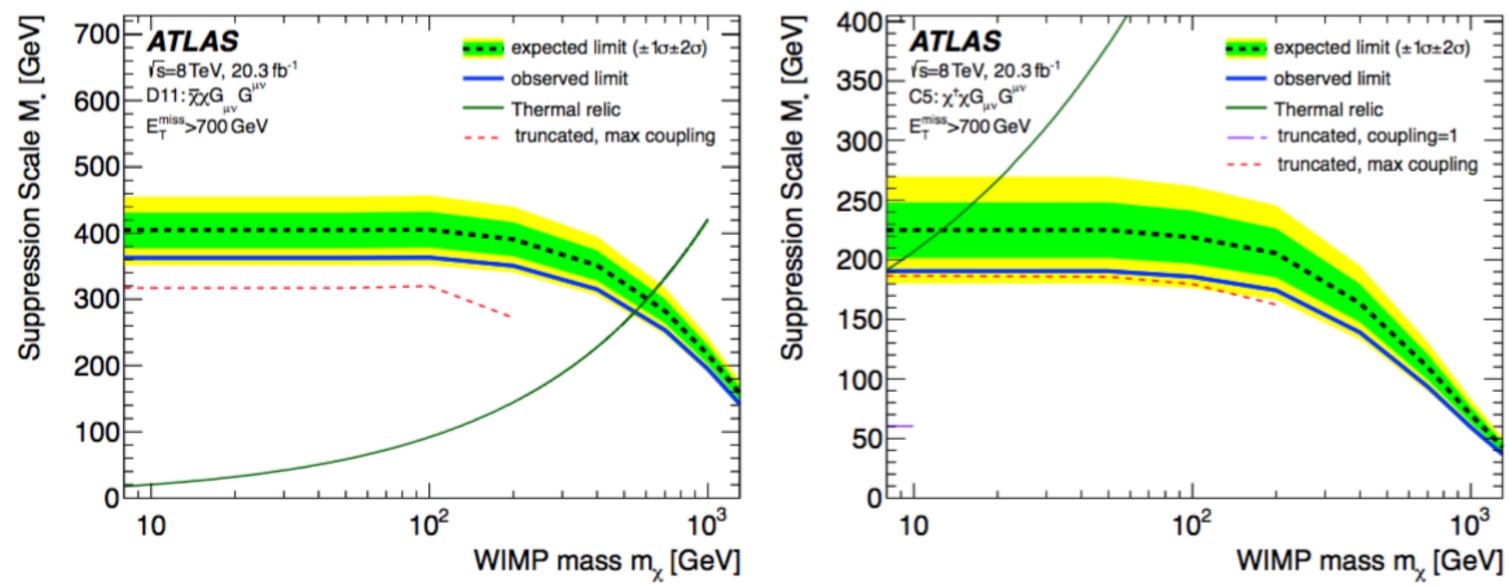

D11 C5

Constraints on Mediator Mass

- Solid lines indicate constant coupling product lines
- For the simplified massive mediator, we find that only at a mediator mass of 10 TeV do we find absolute equality between contact interaction and simplified massive mediator
- At low mediator mass, production is suppressed as WIMP becomes heavier than mediator
- Around the mediator mass, resonant production occurs for narrow resonances

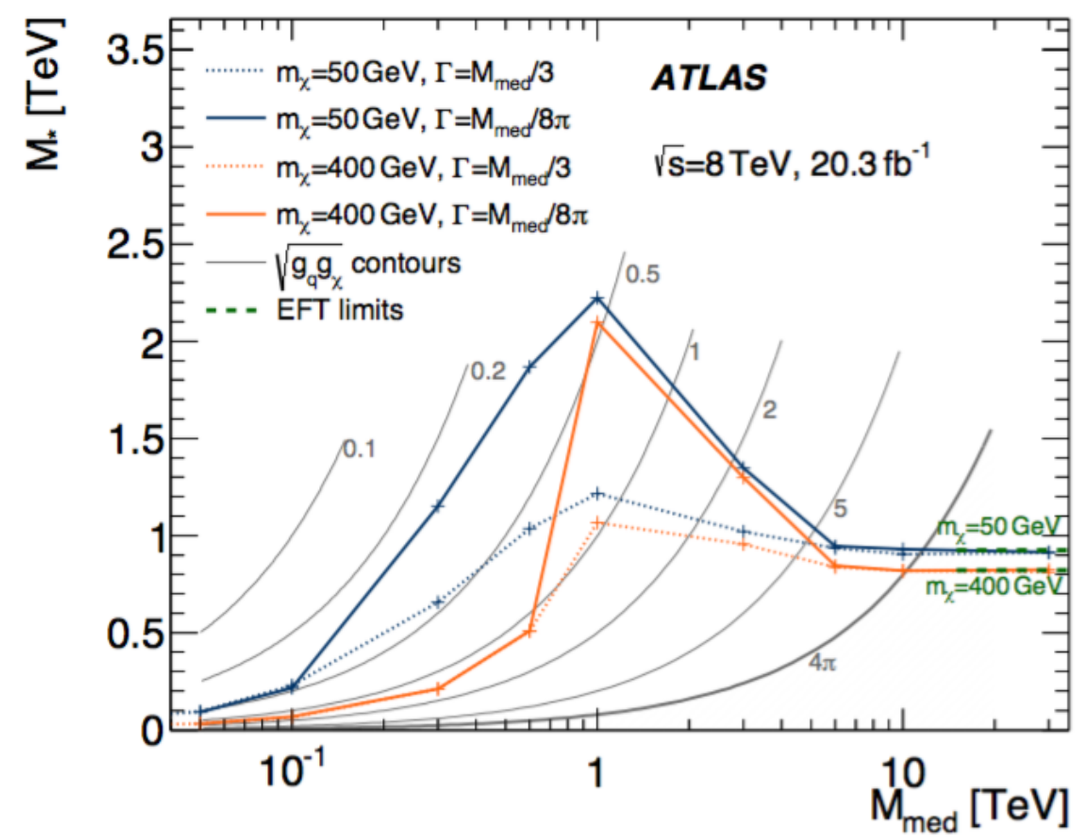

Constraints on Coupling Strength

- Upper left hand corner is the region allowed for relic abundance
- Constraints are not incredibly tight, and very weak for the heaviest mediators
- There is still a lot of “natural” parameter space left, especially in the less explored low-mass region
- Relic abundance ruled out for light mediators, and unlikely for the lowest masses; WIMPless dark matter more preferred by this study

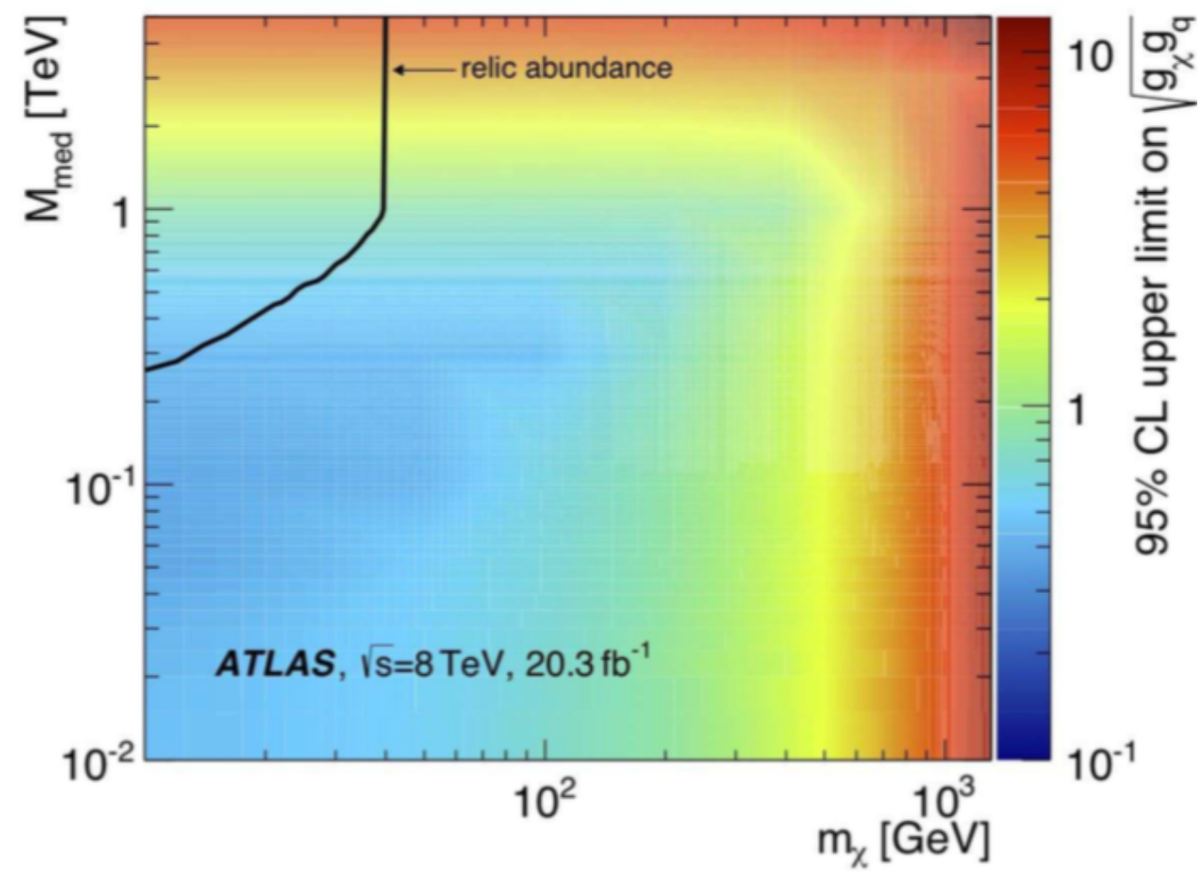

Spin Independent Scattering Limits

- D11 (Gluon Dirac operator) has the only competitive limit above 10 GeV
- Below ~3 GeV, all collider operators have leading limit in the spin-independent space
- C5 increases tension with DAMA signal regions
- As all operators are not below potential reasons, they can't truly rule out proposed signals, only restrict potential couplings which explain them

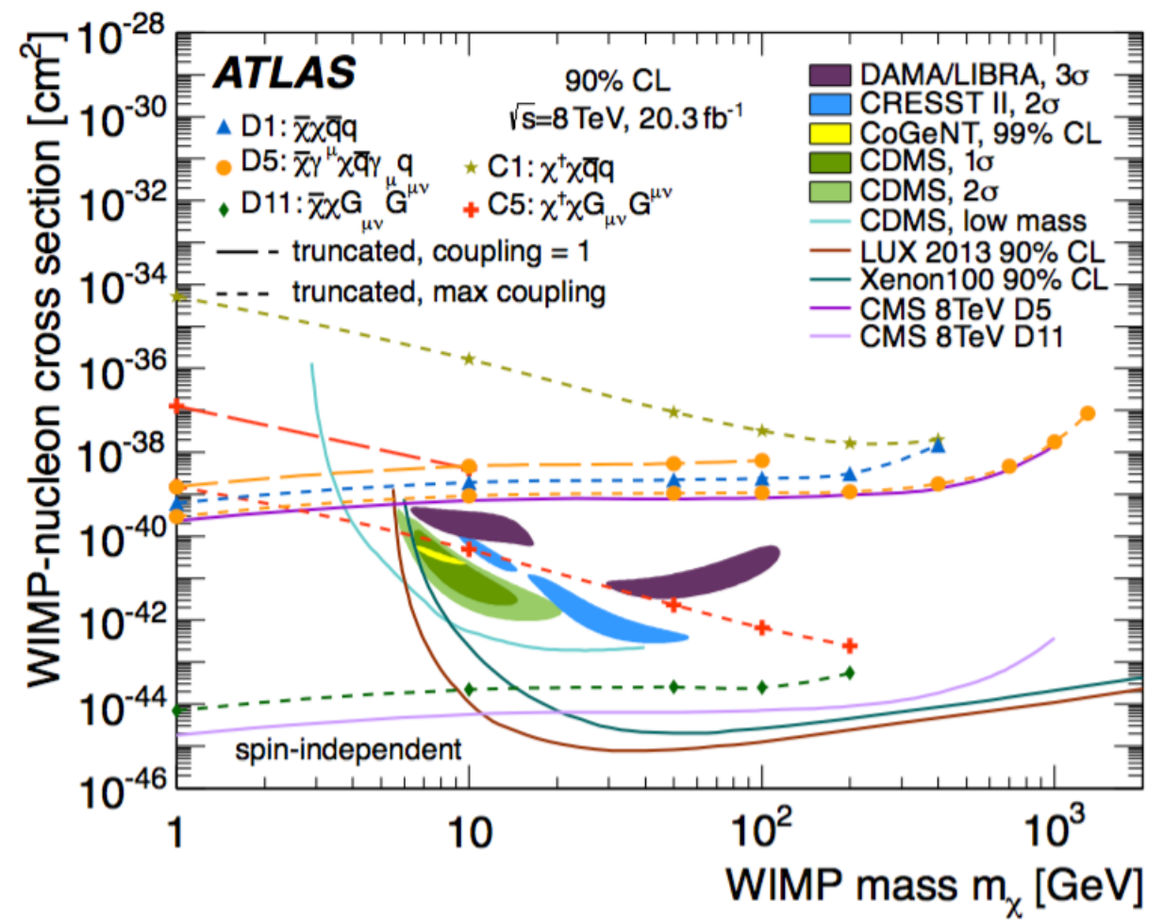

Spin Dependent Scattering Limits

- Spin-dependent limits are much more competitive, leading space across all masses
- ATLAS limits are more competitive with CMS limits in the spin-dependent space
- Colliders again set leading constraints at low WIMP mass due to higher statistics and less dependence on energy thresholds

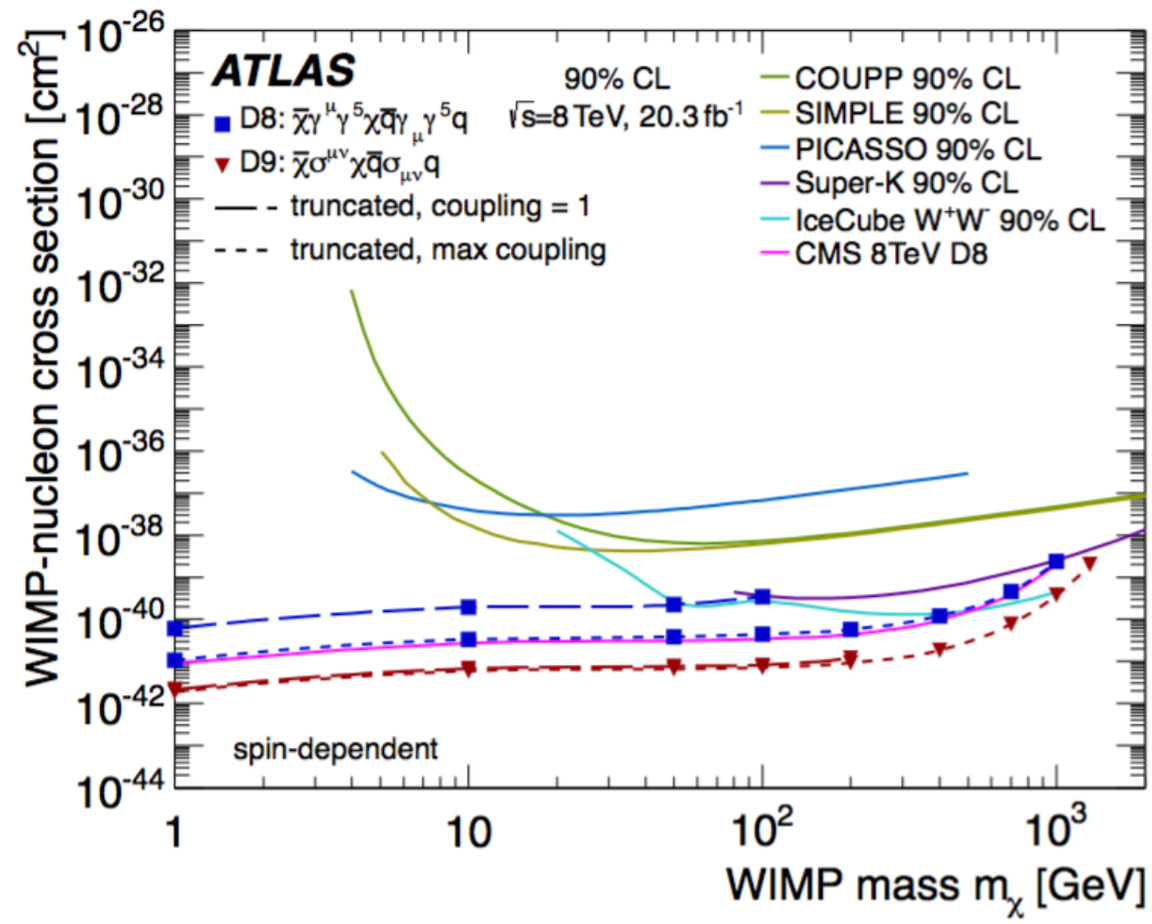

WIMP Annihilation Limits

- Collider constraints in annihilation space are also very competitive, as indirect searches are much more background limited
- This does not include limits from potential lines; may be an outdated comparison
- Truncated coupling are weaker and reduce overall limits at high mass
- We again see tension with relic density unless WIMPs are higher masses

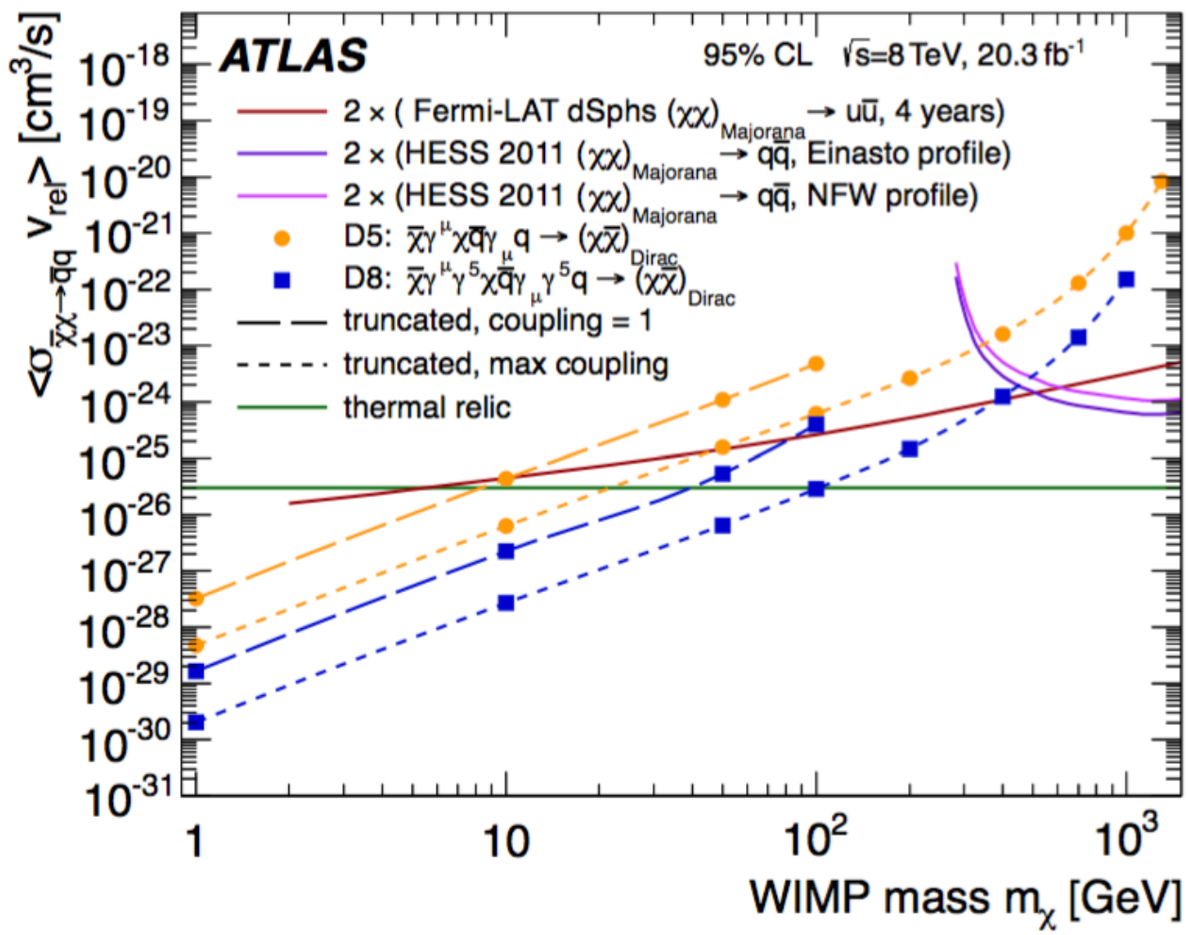

Conclusions

- Monojet analysis sees no excess at 20 inverse femtobarns luminosity with CM energy of 8 TeV
- Mediator masses excluded below ~500 GeV in most cases, with spin-independent limits weakest for Dirac quark couplings, and spin-dependent Dirac couplings strongest
  - Limits scale in an opposite manner to direct detection due to natural spin suppression
- Relic density argument weakened at low WIMP mass, high WIMP mass parameter space still allowable but less attractive for many operators
- Limits still close to EFT breakdown scale; suggests that a new massive mediator around 500 GeV, if found, could change dark matter story at the LHC

Looking Forward: Run 2 Prospects

- CM Energy Roughly doubled; cross-section should increase by ~16 (q^4) for Dirac operators and ~8 for scalar operators
- Increased CM energy also increases the rate by ~4, so we can expect up to 2 orders of magnitude increase in best case
- Remaining parameter space for the “WIMP miracle” is within the reach of Run 2 for Dirac WIMP DM
- Spin-independent Dirac limits will add additional tension to CoGent and DAMA claims for Dirac WIMPs
- Spin-dependent signals are already dominant, but will additionally confirm higher mass limits from indirect detection experiments, and further reduce ability to explain thermal relic abundance

References

(1) ATLAS Collaboration. *Search for new phenomena in final states with an energetic jet and large missing transverse momentum in pp collisions at TeV with the ATLAS detector.* European Physical Journal C, 75:299, July 2015.

(2) J. Goodman, M. Ibe, A. Rajaraman, W. Shepherd, T. M. P. Tait, and H.-B. Yu. *Constraints on dark matter from colliders*. Phys. Rev. D, 82(11):116010, December 2010.

(3) M. Beltran, D. Hooper, E. W. Kolb, Z. A. C. Krusberg, T. M. P. Tait. *Maverick dark matter at colliders.* JHEP 1009 (2010) 037, September 2010

(4) O. Buchmuller, M. Dolan, C. McCabe. *Beyond Effective Field Theory for Dark Matter Searches at the LHC*. JHEP 1401 (2014) 025, January 2014

Backup Slides

Lorentz Invariance of Weyl Fermions

The bilinear term $\bar{\psi}\psi$ is said to be Lorentz invariant because each term is a Dirac fermion which contains left and right handed Weyl fermions:

$$\psi = \begin{pmatrix} \psi_L \\ \psi_R \end{pmatrix}, \ \bar{\psi} = \begin{pmatrix} \psi_R^\dagger, \ \psi_L^\dagger \end{pmatrix}$$

Weyl fermions represent spin 1/2 representations of the Lorentz group, where the left handed fermion is the (1/2,0) representation, and the right handed fermion is the (0,1/2) representation. These transform as

$$\delta\psi_L = \frac{1}{2}(i\theta_i + \beta_i)\sigma_i\psi_L \quad \delta\psi_L^\dagger = \frac{1}{2}(-i\theta_i + \beta_i)\psi_L^\dagger\sigma_i$$

$$\delta\psi_R = \frac{1}{2}(i\theta_i - \beta_i)\sigma_i\psi_R \quad \delta\psi_R^\dagger = \frac{1}{2}(-i\theta_i - \beta_i)\psi_L^\dagger\sigma_i$$

Such that complex mixed chirality bilinear are Lorentz invariants:

$$\delta(\psi_R^\dagger\psi_L) = \psi_R^\dagger\left[\frac{1}{2}(-i\theta_i - \beta_i)\sigma_i^\dagger\right]\psi_L + \psi_R^\dagger\left[\frac{1}{2}(i\theta_i + \beta_i)\sigma_i\right]\psi_L = 0$$

They are complex, though zero, so true Lorentz scalars sum the hermitian conjugates, so that the real Lorentz scalar is

$$\bar{\psi}\psi = \psi_R^\dagger\psi_L + \psi_L^\dagger\psi_R$$

as speculated.

Dirac versus Majorana Fermions

Majorana fermions are a constrained class of Dirac fermions which are invariant under charge conjugation, as a result of being Grassman numbers, which anti-commute. The result of this constraint is that we can express right handed fermions as

$$\psi_R = -i\sigma_2\psi_L^*$$

which gives the Dirac spinor and conjugate

$$\psi = \begin{pmatrix} \psi_L \\ -i\sigma_2\psi_L^* \end{pmatrix}, \ \bar{\psi} = \left(i\sigma_2^\dagger\psi_L^T, \ \psi_L^\dagger,\right)$$

giving the Lorentz invariant Lagrangian

$$\mathcal{L} = i\psi_L\sigma_\mu\partial_\mu\psi_L + i\frac{m}{2}\left(\psi_L^\dagger\sigma_2\psi_L^* - \psi_L^T\sigma_2\psi_L\right)$$

This also tells us that Majorana fermions cannot have charge (otherwise they would violate the U(1) gauge symmetry):

$$\psi_L^T\sigma_2\psi_L \rightarrow \psi_L^T e^{i\alpha}\sigma_2 e^{i\alpha}\psi_L = e^{2i\alpha}\psi_L^T\sigma_2\psi_L$$

The implication of this for our EFT is that assumption of Dirac fermions contains Majorana solutions implicitly, though many of the individual terms become degenerate and any existing couplings are boosted

Dark Matter Collider EFT (Goodman et. al.)

- Assumptions:
  - Only one WIMP in addition to SM particles, only one mediator in addition to gauge bosons, no WIMP coupling to other gauge bosons
  - WIMP odd under some complex symmetry, so invariants must even number of WIMPs
  - WIMP can be a scalar (real or complex) or a Dirac fermion (spins > 1/2 are highly model dependent)

- Complete EFT constructed by enumerating all quark/gluon operators which satisfy these conditions and are not suppressed by extra factors of momentum/mediator mass
  - All Scalars can have scalar or pseudo scalar couplings
  - Complex scalars can use derivatives to add Lorentz invariant vector couplings
  - Fermions can also include vector couplings through use of the Dirac gamma matrices, as well tensor couplings to quarks
  - Two color field strength bilinears are included, without additional derivative couplings which are suppressed
  - Couplings with derivatives are largely suppressed in the low-energy limit, and are excluded in most cases

Name	Operator
D1	$\bar{\chi}\chi\bar{q}q$
D2	$\bar{\chi}\gamma^5\chi\bar{q}q$
D3	$\bar{\chi}\chi\bar{q}\gamma^5 q$
D4	$\bar{\chi}\gamma^5\chi\bar{q}\gamma^5 q$
D5	$\bar{\chi}\gamma^\mu\chi\bar{q}\gamma_\mu q$
D6	$\bar{\chi}\gamma^\mu\gamma^5\chi\bar{q}\gamma_\mu q$
D7	$\bar{\chi}\gamma^\mu\chi\bar{q}\gamma_\mu\gamma^5 q$
D8	$\bar{\chi}\gamma^\mu\gamma^5\chi\bar{q}\gamma_\mu\gamma^5 q$
D9	$\bar{\chi}\sigma^{\mu\nu}\chi\bar{q}\sigma_{\mu\nu}q$
D10	$\bar{\chi}\sigma_{\mu\nu}\gamma^5\chi\bar{q}\sigma_{\alpha\beta}q$
D11	$\bar{\chi}\chi G_{\mu\nu}G^{\mu\nu}$
D12	$\bar{\chi}\gamma^5\chi G_{\mu\nu}G^{\mu\nu}$
D13	$\bar{\chi}\chi G_{\mu\nu}\tilde{G}^{\mu\nu}$
D14	$\bar{\chi}\gamma^5\chi G_{\mu\nu}\tilde{G}^{\mu\nu}$
C1	$\chi^\dagger\chi\bar{q}q$
C2	$\chi^\dagger\chi\bar{q}\gamma^5 q$
C3	$\chi^\dagger\partial_\mu\chi\bar{q}\gamma^\mu q$
C4	$\chi^\dagger\partial_\mu\chi\bar{q}\gamma^\mu\gamma^5 q$
C5	$\chi^\dagger\chi G_{\mu\nu}G^{\mu\nu}$
C6	$\chi^\dagger\chi G_{\mu\nu}\tilde{G}^{\mu\nu}$
R1	$\chi^2\bar{q}q$
R2	$\chi^2\bar{q}\gamma^5 q$
R3	$\chi^2 G_{\mu\nu}G^{\mu\nu}$
R4	$\chi^2 G_{\mu\nu}\tilde{G}^{\mu\nu}$

Table from Ref. 2 (Goodman et. al. 2010)

Dark Matter Collider EFT (Goodman et. al.)

- Coefficients are chosen starting from tree-level diagrams. The units of the coefficients must allow the terms to have overall mass dimension 4
- Quark mass is included in the scalar couplings to provide an easier comparison to direct-detection operators; it also removes effects from flavor-changing neutral currents
- Additional strong coupling term added to account for loop contribution in gluon terms, which require one loop for gluon-gluon fusion (as in ttbar and Higgs production)
- From these vertices we can 6 classes of terms which will have similar spectral properties in this EFT:
  - D1-D4
  - D5-D8, C3-C4
  - D9-D10
  - D11-D14
  - C1-C2, R1-R2
  - C5-C6, R3-R4

Name	Operator	Coefficient
D1	$\bar{\chi}\chi\bar{q}q$	m_q/M_*^3
D2	$\bar{\chi}\gamma^5\chi\bar{q}q$	im_q/M_*^3
D3	$\bar{\chi}\chi\bar{q}\gamma^5 q$	im_q/M_*^3
D4	$\bar{\chi}\gamma^5\chi\bar{q}\gamma^5 q$	m_q/M_*^3
D5	$\bar{\chi}\gamma^\mu\chi\bar{q}\gamma_\mu q$	$1/M_*^2$
D6	$\bar{\chi}\gamma^\mu\gamma^5\chi\bar{q}\gamma_\mu q$	$1/M_*^2$
D7	$\bar{\chi}\gamma^\mu\chi\bar{q}\gamma_\mu\gamma^5 q$	$1/M_*^2$
D8	$\bar{\chi}\gamma^\mu\gamma^5\chi\bar{q}\gamma_\mu\gamma^5 q$	$1/M_*^2$
D9	$\bar{\chi}\sigma^{\mu\nu}\chi\bar{q}\sigma_{\mu\nu}q$	$1/M_*^2$
D10	$\bar{\chi}\sigma_{\mu\nu}\gamma^5\chi\bar{q}\sigma_{\alpha\beta}q$	i/M_*^2
D11	$\bar{\chi}\chi G_{\mu\nu}G^{\mu\nu}$	$\alpha_s/4M_*^3$
D12	$\bar{\chi}\gamma^5\chi G_{\mu\nu}G^{\mu\nu}$	$i\alpha_s/4M_*^3$
D13	$\bar{\chi}\chi G_{\mu\nu}\tilde{G}^{\mu\nu}$	$i\alpha_s/4M_*^3$
D14	$\bar{\chi}\gamma^5\chi G_{\mu\nu}\tilde{G}^{\mu\nu}$	$\alpha_s/4M_*^3$
C1	$\chi^\dagger\chi\bar{q}q$	m_q/M_*^2
C2	$\chi^\dagger\chi\bar{q}\gamma^5 q$	im_q/M_*^2
C3	$\chi^\dagger\partial_\mu\chi\bar{q}\gamma^\mu q$	$1/M_*^2$
C4	$\chi^\dagger\partial_\mu\chi\bar{q}\gamma^\mu\gamma^5 q$	$1/M_*^2$
C5	$\chi^\dagger\chi G_{\mu\nu}G^{\mu\nu}$	$\alpha_s/4M_*^2$
C6	$\chi^\dagger\chi G_{\mu\nu}\tilde{G}^{\mu\nu}$	$i\alpha_s/4M_*^2$
R1	$\chi^2\bar{q}q$	$m_q/2M_*^2$
R2	$\chi^2\bar{q}\gamma^5 q$	$im_q/2M_*^2$
R3	$\chi^2 G_{\mu\nu}G^{\mu\nu}$	$\alpha_s/8M_*^2$
R4	$\chi^2 G_{\mu\nu}\tilde{G}^{\mu\nu}$	$i\alpha_s/8M_*^2$

Table from Ref. 2 (Goodman et. al. 2010)

Scattering Rate and Luminosity

- We can write the scattering rate as the product of luminosity (events per second per Area) times cross section, giving total events in terms of integrated luminosity:

$$\frac{dN}{dt} = \sigma L \rightarrow N = \sigma L_{int}$$

- Integrated luminosity thus has dimensions of 1/cm^2 to leave N dimensionless. This is typically expressed in inverse fb (femtobarns), where a barn is the cross-section of a uranium nucleus:

$$1 fb^{-1} = 10^{39}\ cm^{-2}$$

- Thus for a luminosity of 1 inverse femtobarn, we expect one event per femtobarn of cross-section

Single Electron Control Region

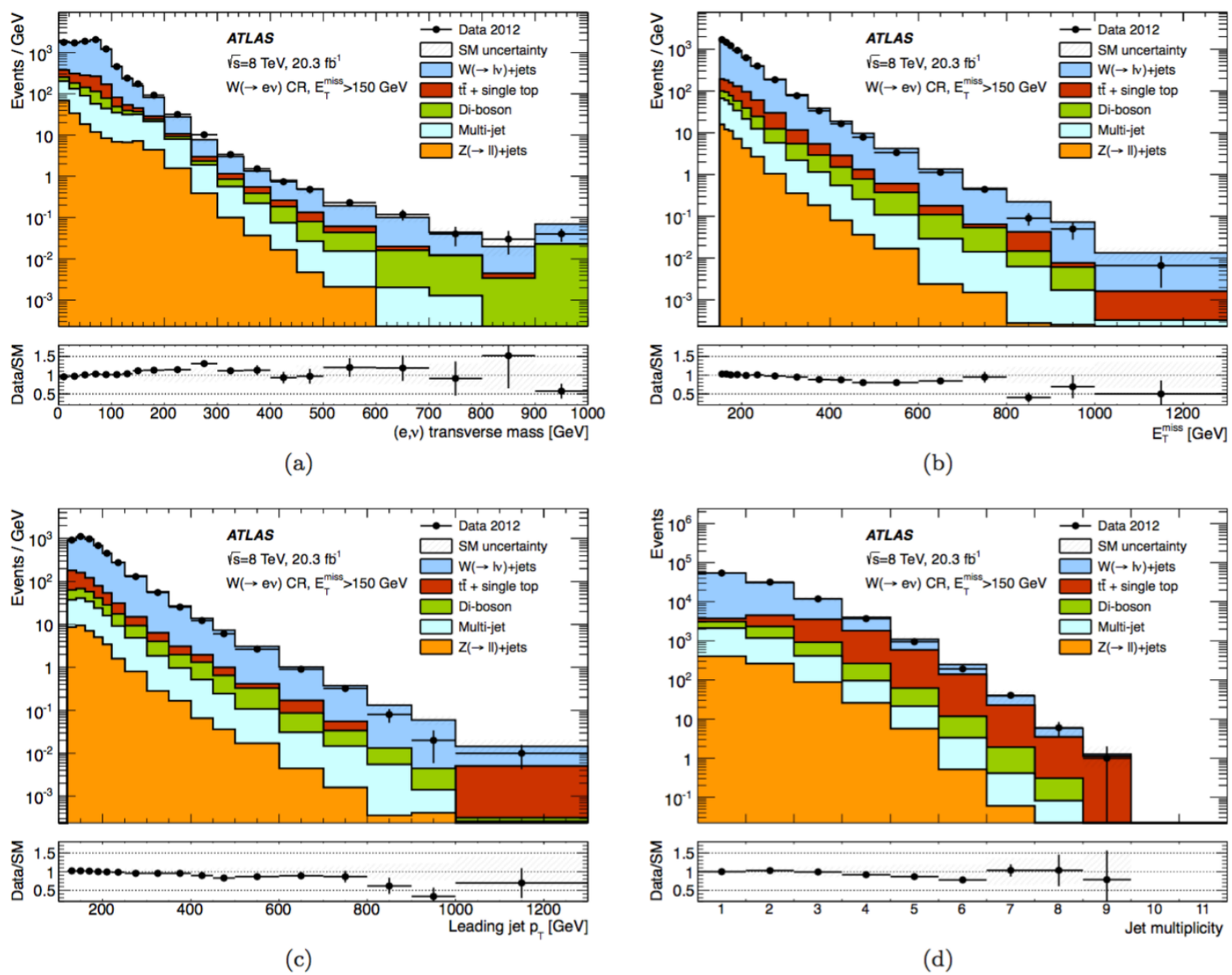

Fig. 4 Distributions of the measured (a) transverse mass of the identified electron and the missing transverse momentum, (b) $E_{\mathrm{T}}^{\mathrm{miss}}$, (c) leading jet p_{T} and (d) jet multiplicity distributions in the $W(\rightarrow e\nu)$+jets control region for the inclusive SR1 selection, compared to the background expectations. The latter include the global normalization factors extracted from the data. Where appropriate, the last bin of the distribution includes overflows. The lower panels represent the ratio of data to MC expectations. The error bands in the ratios include the statistical and experimental uncertainties on the background expectations.

Multiple Electron Control Region

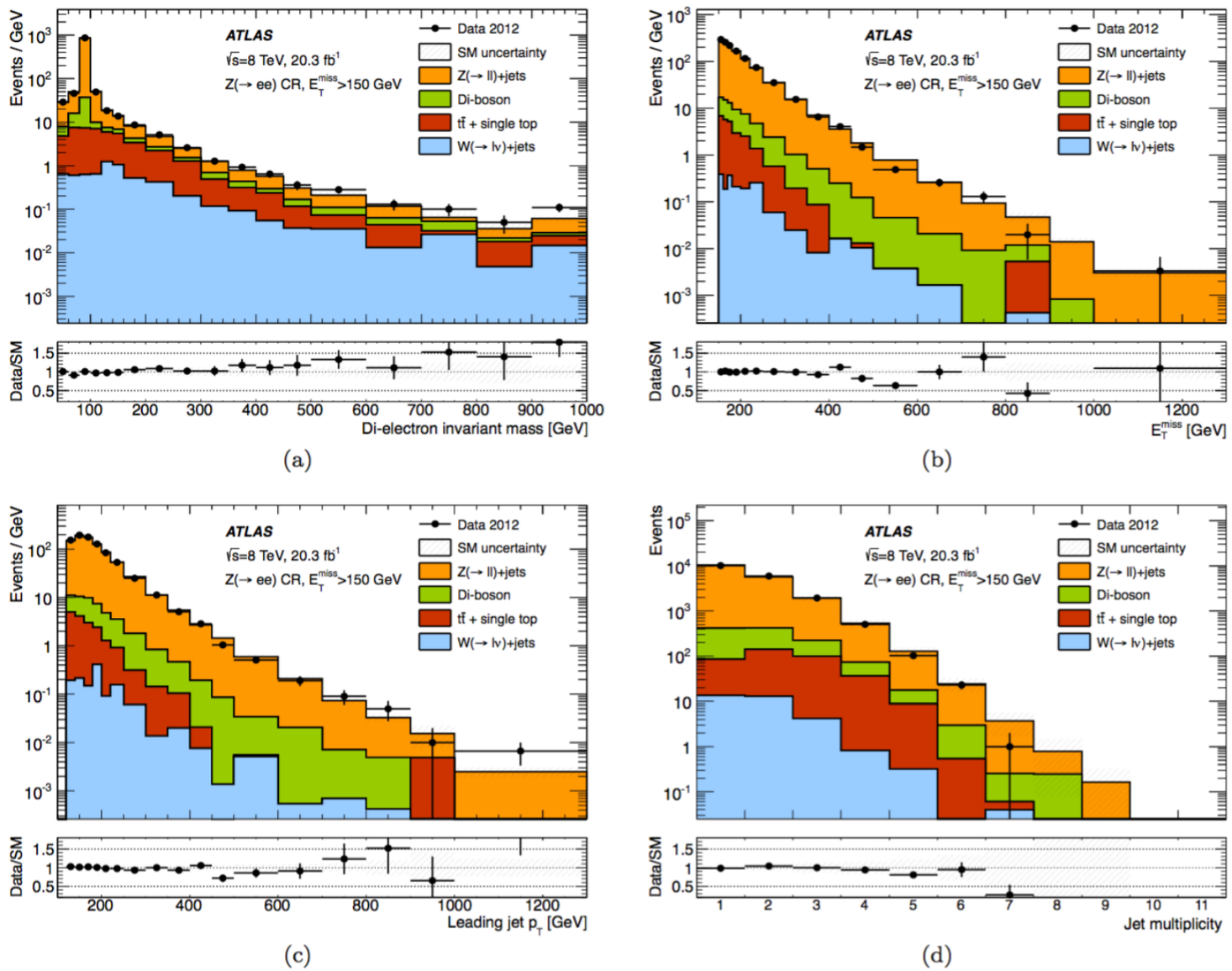

Fig. 5 Distributions of the measured (a) dilepton invariant mass, (b) $E_{\mathrm{T}}^{\mathrm{miss}}$, (c) leading jet p_{T} and (d) jet multiplicity distributions in the $Z/\gamma^*(\rightarrow e^+e^-)$+jets control region for the inclusive SR1 selection, compared to the background expectations. The latter include the global normalization factors extracted from the data. Where appropriate, the last bin of the distribution includes overflows. The lower panels represent the ratio of data to MC expectations. The error bands in the ratios include the statistical and experimental uncertainties on the background expectations.